Yellow InCl as a distorted rock-salt lattice

1997 J. Phys.: Condens. Matter 9 9759

(http://iopscience.iop.org/0953-8984/9/45/006)

J. Phys.: Condens. Matter **9** (1997) 9759–9783. Printed in the UK PII: S0953-8984(97)83982-3

Yellow InCl as a distorted rock-salt lattice

W J A Maaskant

Leiden Institute of Chemistry, Gorlaeus Laboratories, PO Box 9502, 2300 RA Leiden, The Netherlands

Received 7 May 1997

Abstract. Because of the subgroup–group relationship which exists between the space group of yellow InCl ($P2_13, Z = 32$) and that of rock salt ($Fm\bar{3}m, Z = 1$), a Landau expansion of the free energy in invariants of the symmetry group of higher order can be performed and a mechanism for distortion arises. The special feature of this hypothetical phase transition is that three lattice modes of different symmetry type and of almost equal force constant bring about the deformation. These three modes, which are apparently nearly degenerate, effect longitudinal displacements of rows of ions, with different amplitudes for the cations and the anions. When these are described by an order parameter, an expansion of the free energy up to the fourth power and containing third-order terms is possible. The cooperation of pseudo-degenerate modes of different symmetry is a hitherto unknown distortion mechanism. Yellow InCl is further characterized by bilinear quantities describing ferrodistortive chirality (A_{1u}) and electric 'A_{2u}' octupoles and antiferrodistortive spiral (A_{2g}) arrangements. These bilinear quantities are related to fourth-order Landau invariants. Yellow InCl has an electric octupole lattice. In addition, on the basis of the analogy with optical rotatory power, new mechanisms of this effect are predicted.

1. Introduction

The crystal structure of yellow InCl was determined for the first time by Van den Berg [1, 2] and was redetermined by Van der Vorst *et al* [3]. Yellow InCl has a complicated structure with space group (S.G.) $P2_13$ and $Z = 32$. The structure is unique, in the sense that no other compound is known to have this structure. From the structure determinations [1–3] it has already become clear that this space group is a subgroup of the group $Fm\bar{3}m$ of rock salt (also referred to as the B1 structure type). Van den Berg used the rock-salt positions as a starting point for the structure derivation. We will give a table *vide infra* which shows the differences between the real ion positions and those of a rock-salt-like structure. However, no phase transition between the yellow InCl phase and a rock-salt structure has ever been found. Above 390 K a red form of InCl is stable. It has the β-TlI structure (S.G. $Cmcm, Z = 4$) [3], which is known to occur in several other compounds. There is no subgroup–group relationship between $Cmcm$ and the space groups of rock salt and of yellow InCl.

The distortion from the B1-type structure has been attributed to the presence of a $5s^2$ outer-electron configuration in the In^+ ion [4, 5]. In general these lone pairs of the more general type ns^2 occur on lower-valence cations of the p-block elements. A variety of local coordinations occur among simple AB compounds, where A represents such a cation. For example PbS, PbSe and PbTe all have the rock-salt structure [6] with 6-coordination. On the other hand TlCl, TlBr and α-TlI each have a CsCl-like (B2-type, 8-coordination) structure [6]. α-GeTe shows trigonally distorted octahedra (S.G. $R3m, Z = 1$) [7]. Its space group

0953-8984/97/459759+25$19.50

is a subgroup of $Fm\bar{3}m$. It is a well-known ferroelectric and its phase transition to the B1-type structure is described in several places (see, e.g., [8]). Also β-TlF [9] and β-PbO [10, 11] show deformed B1 structures. Furthermore, in red InCl (with the β-TlI structure), in one direction double layers of the rock-salt type are still observable; see, e.g., [12, 13]. This evidence supports the fundamental idea that the supergroup with respect to the space group of yellow InCl is the space group of rock salt. The unit cell of (yellow) InCl is a cube with cell parameters twice as large as the cubic cell parameters of the underlying B1 structure. The index between the two space groups is 128, which is exceptionally large.

The distortions of the $InCl_6$ octahedra due to the stereochemically active $5s^2$ lone pairs in the structures of yellow InCl and red InCl have been studied by us in two papers: Van der Vorst and Maaskant [4] and Maaskant [5]. These papers also give diagrams of the local octahedra. But a diagram of the lattice distortion as a whole has never been published since, up to now, the essence of the cooperative deformation has not been understood.

It is the aim of the present paper to explain the mechanism of the lattice distortion. It will be shown that to a good approximation the lattice deformation is a superposition of three equally strong modes belonging to different irreducible representations of the space group $Fm\bar{3}m$. This will result in a pattern of longitudinal shifts of rows of ions (figures 8 and 9—see later).

Since the space group of yellow InCl is a subgroup of the space group of rock salt, it is possible to develop the thermodynamic potential (often called the free energy) in a series containing invariants of the higher space group. Such series have been used by Landau [14] (also Landau and Lifshitz [15]) in order to formulate the conditions for a second-order phase transition. In the case of a second-order phase transition the order parameter can in principle be made infinitely small, in order to ensure convergence of the series expansion. In the case of InCl we have no phase transition, and a strict proof that such a development can be cut off after the fourth power of the order parameters is lacking. However, this assumption does not lead to absurdities. Not only has no phase transition to or from the rock-salt structure been found, but also there is no experimental evidence of a successive series of phase transitions, such as occurs sometimes for other compounds.

Van der Vorst [16] expressed the shifts of the ions in InCl with respect to the rock-salt structure positions in terms of lattice modes of the high-symmetry S.G. ($Fm\bar{3}m$). A derivation of these lattice modes has never been given before, and will be described in the appendix (section A.1). Section 2 introduces the 'geometric' approximation and the local distortion coordinates.

Section 3 shows that the geometric approximation is characterized by distortions which resemble isolated longitudinal shifts of rows of ions. Three lattice modes of different symmetries and almost equal amplitudes determine these longitudinal shifts. The harmonic energies of these three modes are estimated to be approximately equal. Diagrams of the displacements of each type of mode are given, as well as of their combination for the 'geometric' approximation. Also the possibility of a new type of optical chirality is indicated.

In section 4 the third-order invariants in the development of the free energy are derived. As third-order invariants are definitely there, the hypothetical phase transition would be of the first order, since the third Landau condition has not been fulfilled.

In section 5 the fourth-order Landau invariants in the development of the free energy are derived. A new method is used in trying to deduce from the reduction of the point group of the crystal whether there are bilinear quantities which belong to the Γ point. In yellow InCl, these bilinear quantities clarify the resulting deformations. Whereas the Δ modes are responsible for the ferrodistortive chirality, which arises from two sources, the

W modes are responsible for a ferrodistortive ordering of tetrahedral octupoles, also from two origins. The Σ_4 normal mode induces antiferrodistortively ordered bilinear quantities of 'A_{2g}' symmetry. The number of fourth-order invariants is large.

In section 6 the Landau expansion of the free energy of the hypothetical phase transition is given. What differs in our treatment from other cases is that the second Landau condition is not fulfilled. We state that three pseudo-degenerate modes of equal strength and belonging to different irreducible representations (in the following shortened to irreps) describe the cooperative distortion in yellow InCl to a good approximation.

In this paper, very often scalar products are applied. We discriminate between scalars that are totally symmetric in the point group $m\bar{3}m$ and those that belong to one-dimensional irreps other than A_{1g}. The latter are called pseudoscalars.

Table 1. Deviations in yellow InCl from the idealized B1 positions given as fractions of the cubic cell parameter.

Ion	x_0	y_0	z_0	δ_x	δ_y	δ_z
In(1)	$\frac{1}{4}$	$\frac{1}{4}$	0	−0.0013	−0.0302	−0.0288
In(2)	$\frac{3}{4}$	$\frac{3}{4}$	0	0.0027	0.0281	0.0295
In(3)	0	0	0	0.0302	0.0302	0.0302
In(4)	$\frac{1}{2}$	$\frac{1}{2}$	$\frac{1}{2}$	−0.0327	−0.0327	−0.0327
Cl(1)	$\frac{1}{4}$	0	0	0.0505	−0.0504	0.0005
Cl(2)	$\frac{3}{4}$	0	0	0.0498	0.0549	−0.0110
Cl(3)	$\frac{1}{4}$	$\frac{1}{4}$	$\frac{1}{4}$	−0.0439	−0.0439	−0.0439
Cl(4)	$\frac{3}{4}$	$\frac{3}{4}$	$\frac{3}{4}$	0.0486	0.0486	0.0486

2. Symmetrized deformations

Table 1 expresses the experimental distortions from the B1 structure [3]. The rock-salt positions, expressed in the space group of yellow InCl, are given in the columns headed by x_0, y_0, z_0. The deviations (δ_x, δ_y, δ_z) are an order of magnitude smaller than the rock-salt values, giving further evidence of the subgroup–group relationship between yellow InCl and the B1 structure.

Table 1 also shows that there are different types of site in the unit cell of InCl. In(1), In(2), Cl(1) and Cl(2) are at a general point, which is twelvefold. In(3), In(4), Cl(3) and Cl(4) lie on threefold axes and are fourfold.

Van der Vorst [16] has expressed these deformations in lattice symmetry coordinates. Since we use differently normalized symmetry modes (see table A1, later) our results (table 2) differ. The primed symbols denote the In ions, while the unprimed symbols denote the Cl ions. The precision of these numbers is the same as that for the parameters found from the crystal structure determination [3].

Table 2 shows that some of the symmetry coordinates are very small while the others are almost equal in absolute value both for the In and the Cl ions. In table 3 we give the parameters for what we call the 'geometric' approximation. We have taken one linear combination with equal absolute amplitudes for the two Δ modes and similarly for the W modes. Since the Σ_4 mode is single, the absolute values of s_3 and s_3' are $\sqrt{2}$ larger than the absolute values of the Δ and W parameters. The 'geometric' approximation consists in

allocating the combination of Δ modes, the combination of W modes and the Σ_4 mode the same absolute amplitude.

Table 4 shows the coordinates of the 'geometric' approximation given as fractions of the cell parameter of yellow InCl and the differences (u_x, u_y and u_z) from the observed values. Note that the latter are in general an order of magnitude smaller than the differences from the rock-salt structure. We discuss in the following only this idealized form for InCl. It has the same space group as yellow InCl.

Table 2. Experimental symmetry coordinates.

$d'_1 = 0.0197$	$s'_1 = -0.0001$	$d_1 = 0.0272$	$s_1 = -0.0001$
$d'_2 = -0.0191$	$s'_2 = -0.0014$	$d_2 = -0.0248$	$s_2 = 0.0028$
$w'_1 = 0.0188$	$s'_3 = -0.0252$	$w_1 = -0.0342$	$s_3 = -0.0456$
$w'_2 = 0.0166$	$l'_1 = -0.0002$	$w_2 = 0.0318$	$l_2 = 0.0002$

Table 3. Symmetry coordinates for the 'geometric' approximation.

$d'_1 = 0.0184$	$s'_1 = 0.0000$	$d_1 = 0.0300$	$s_1 = 0.0000$
$d'_2 = -0.0184$	$s'_2 = 0.0000$	$d_2 = -0.0300$	$s_2 = 0.0000$
$w'_1 = 0.0184$	$s'_3 = -0.0260$	$w_1 = -0.0300$	$s_3 = -0.0425$
$w'_2 = 0.0184$	$l'_1 = 0.0000$	$w_2 = 0.0300$	$l_2 = 0.0000$

Table 4. The coordinates arising from the 'geometric' approximation and the deviations of the observed coordinates (the last three columns).

Ion	x_0	y_0	z_0	δ_x	δ_y	δ_z	u_x	u_y	u_z
In(1)	$\frac{1}{4}$	$\frac{1}{4}$	0	0.0000	−0.0301	−0.0301	−0.0013	−0.0001	0.0013
In(2)	$\frac{3}{4}$	$\frac{3}{4}$	0	0.0000	0.0301	0.0301	0.0027	−0.0020	−0.0006
In(3)	0	0	0	0.0301	0.0301	0.0301	0.0001	0.0001	0.0001
In(4)	$\frac{1}{2}$	$\frac{1}{2}$	$\frac{1}{2}$	−0.0301	−0.0301	−0.0301	−0.0026	−0.0026	−0.0026
Cl(1)	$\frac{1}{4}$	0	0	0.0491	−0.0491	0.0000	0.0014	−0.0013	0.0000
Cl(2)	$\frac{3}{4}$	0	0	0.0491	0.0491	0.0000	0.0007	0.0058	−0.0115
Cl(3)	$\frac{1}{4}$	$\frac{1}{4}$	$\frac{1}{4}$	−0.0491	−0.0491	−0.0491	0.0052	0.0052	0.0052
Cl(4)	$\frac{3}{4}$	$\frac{3}{4}$	$\frac{3}{4}$	0.0486	0.0486	0.0486	−0.0005	−0.0005	−0.0005

The local distortion modes of a regular octahedron are defined in table A3 of appendix A.2—see later. In table 5 the local distortion coordinates of the deformed Cl octahedra for the four In positions and also the deformed In octahedra for the four Cl positions are given. There are three T_{1u} modes, which can be expected to interact. However, our choice in this table leads to the simplest coordinates. Table 5 shows that In(1) and Cl(1) have one single T_{2u} mode each. Figure 1 shows its z-component. This transforms as $z(x^2 - y^2)$ in $m\bar{3}m$. The mode consists of dipolar moments of the ligands in the z-direction, modulated by $x^2 - y^2$. This is an electric octupole. Since $L = 3$, we expect in a cubic system a decomposition into T_{1u}, T_{2u} and A_{2u}. The z-components of the T_{1u} moments transform as

Table 5. Idealized octahedral symmetry coordinates given as fractions of the cell parameter of InCl $\times 10^4$. The ideal coordinates for the four In sites and the four Cl sites are given in tables A4 and A5, respectively—see later.

	In(1)	In(2)	In(3)	In(4)	Cl(1)	Cl(2)	Cl(3)	Cl(4)
$q(a_{1g})$	0	0	0	0	0	0	0	0
$q(e_{g\theta})$	0	0	0	0	0	0	0	0
$q(e_{g\epsilon})$	0	0	0	0	0	0	0	0
$q(t_{1gx})$	496	496	−496	−496	300	300	−300	−300
$q(t_{1gy})$	496	−496	−496	−496	300	−300	−300	−300
$q(t_{1gz})$	496	496	−496	−496	300	300	−300	−300
$q(t_{2gyz})$	−496	−496	−496	−496	300	300	300	300
$q(t_{2gzx})$	496	−496	−496	−496	300	−300	300	300
$q(t_{2gxy})$	−496	−496	−496	−496	−300	−300	300	300
$q(t_{1u1x})$	300	−300	300	−300	496	−496	−496	496
$q(t_{1u1y})$	300	−300	300	−300	0	0	−496	496
$q(t_{1u1z})$	0	0	300	−300	496	496	−496	496
$q(t_{1u2x})$	701	−701	701	−701	424	−424	−424	424
$q(t_{1u2y})$	701	−701	701	−701	0	0	−424	424
$q(t_{1u2z})$	0	0	701	−701	424	424	−424	424
$q(t_{1u3x})$	0	0	0	0	0	0	0	0
$q(t_{1u3y})$	0	0	0	0	0	−600	0	0
$q(t_{1u3z})$	0	992	0	0	0	0	0	0
$q(t_{2ux})$	0	0	0	0	0	0	0	0
$q(t_{2uy})$	0	0	0	0	−600	0	0	0
$q(t_{2uz})$	992	0	0	0	0	0	0	0

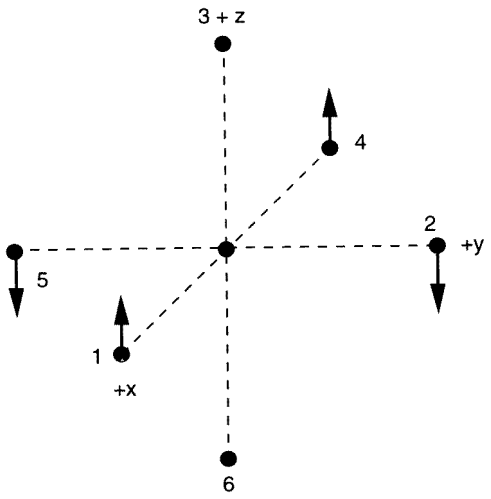

Figure 1. A typical T_{2u} distortion mode.

$z(2z^2 - x^2 - y^2)$. T_{1u} moments are also present in the structure. They are mixed with other types of T_{1u} moment of the octahedra. The A_{2u} component, however, transforms as xyz and is not recognized by the ligands, since these are situated on the cartesian axes where xyz is always zero.

In appendix A.3 scalar invariants for the S.G. $P2_13$ are derived. These can be shown to determine the differences between the In sites or between the Cl sites.

Table 6. The distortion by the $\boldsymbol{k}_6^1$-mode of two columns of ions. The numbers are fractions $\times 10^4$ of the InCl cell parameter.

	$In3_1$	$Cl2_3$	$In4_2$	$Cl2_3$		$Cl1_1$	$In1_3$	$Cl1_{10}$	$In1_{12}$
Position					Position				
x	0	0	0	0	x	2500	2500	2500	2500
y	0	0	0	0	y	0	0	0	0
z	0	2500	5000	7500	z	0	2500	5000	7500
Deviation					Deviation				
dx	150	0	−150	0	dx	248	0	−248	0
dy	0	−248	0	248	dy	0	−150	0	150
dz	0	0	0	0	dz	0	0	0	0
R_x	248	0	−248	0	R_x	150	0	−150	0
R_y	0	−150	0	150	R_y	0	−248	0	248
R_z	0	0	0	0	R_z	0	0	0	0
Q_{yz}	−248	0	248	0	Q_{yz}	−150	0	150	0
Q_{zx}	0	−150	0	150	Q_{zx}	0	−248	0	248
Q_{xy}	0	0	0	0	Q_{xy}	0	0	0	0
$\mu 1_x$	150	0	−150	0	$\mu 1_x$	248	0	−248	0
$\mu 1_y$	0	−248	0	248	$\mu 1_y$	0	−150	0	150
$\mu 1_z$	0	0	0	0	$\mu 1_z$	0	0	0	0
$\mu 2_x$	350	0	−350	0	$\mu 2_x$	212	0	−212	0
$\mu 2_y$	0	−212	0	212	$\mu 2_y$	0	−350	0	350
$\mu 2_z$	0	0	0	0	$\mu 2_z$	0	0	0	0
$\mu 3_x$	248	0	−248	0	$\mu 3_x$	150	0	−150	0
$\mu 3_y$	0	−150	0	150	$\mu 3_y$	0	−248	0	248
$\mu 3_z$	0	0	0	0	$\mu 3_z$	0	0	0	0
F_x	248	0	−248	0	F_x	150	0	−150	0
F_y	0	150	0	−150	F_y	0	248	0	−248
F_z	0	0	0	0	F_z	0	0	0	0

3. Description of the distortion mechanism

In this section we discuss the deformations due to single modes and combinations of distortion waves. The Δ modes will be shown to consist of standing, circularly polarized, planar waves along the (cubic) cell axes. These waves all have the same sense and magnitude of the chirality. The latter can be shown to result in terms such as $\boldsymbol{\mu}\cdot\boldsymbol{R}$, the scalar product of the displacements and rotations, and $\boldsymbol{Q}\cdot\boldsymbol{F}$, where $\boldsymbol{Q}$ represents the quadrupole moments Q_{yz}, Q_{zx}, Q_{xy} and $\boldsymbol{F}$ has components which transform as $x(y^2-z^2)$, $y(z^2-x^2)$, $z(x^2-y^2)$ respectively. These pseudoscalar products will be shown to be present in fourth-order energy terms. In table 6 the action of just $\boldsymbol{k}_6^1$ on two columns of ions arranged along the z-direction is given. For example $Cl1_3$ denotes a Cl ion of type 1 numbered 3 (there are 12 ions of this type in the unit cell). The x, y, z denote fractional coordinates $\times 10^4$ with respect to the InCl unit cell. dx, dy and dz denote the shifts in the x-, y-, z-directions respectively. The other quantities are moments, where R stands for T_{1g}, Q for T_{2g}, μ_1 for T_{1u1} and similarly for the other μ-components, and F means T_{2u}.

Since the $\boldsymbol{k}_6$-modes represent planar waves, a comparison with light waves is easily

Table 7. The distortion by the k_8^1-mode of two columns of ions. The numbers are fractions $\times 10^4$ of the InCl cell parameter.

	$In3_1$	$Cl2_3$	$In4_2$	$Cl2_3$		$Cl1_1$	$In1_3$	$Cl1_{10}$	$In1_{12}$
Position					Position				
x	0	0	0	0	x	2500	2500	2500	2500
y	0	0	0	0	y	0	0	0	0
z	0	2500	5000	7500	z	0	2500	5000	7500
Shift					Shift				
dx	150	0	−150	0	dx	248	0	−248	0
dy	0	248	0	−248	dy	0	−150	0	150
dz	0	0	0	0	dz	0	0	0	0
R_x	−248	0	248	0	R_x	150	0	−150	0
R_y	0	−150	0	150	R_y	0	−248	0	248
R_z	0	0	0	0	R_z	0	0	0	0
Q_{yz}	248	0	−248	0	Q_{yz}	−150	0	150	0
Q_{zx}	0	−150	0	150	Q_{zx}	0	−248	0	248
Q_{xy}	0	0	0	0	Q_{xy}	0	0	0	0
$\mu 1_x$	150	0	−150	0	$\mu 1_x$	248	0	−248	0
$\mu 1_y$	0	248	0	−248	$\mu 1_y$	0	−150	0	150
$\mu 1_z$	0	0	0	0	$\mu 1_z$	0	0	0	0
$\mu 2_x$	350	0	−350	0	$\mu 2_x$	212	0	−212	0
$\mu 2_y$	0	212	0	−212	$\mu 2_y$	0	−350	0	350
$\mu 2_z$	0	0	0	0	$\mu 2_z$	0	0	0	0
$\mu 3_x$	−248	0	248	0	$\mu 3_x$	−150	0	150	0
$\mu 3_y$	0	−150	0	150	$\mu 3_y$	0	248	0	−248
$\mu 3_z$	0	0	0	0	$\mu 3_z$	0	0	0	0
F_x	−248	0	248	0	F_x	−150	0	150	0
F_y	0	150	0	−150	F_y	0	−248	0	248
F_z	0	0	0	0	F_z	0	0	0	0

made. There is a connection between the phenomenon of rotation of the plane of polarization of light and the distortion due to e.g. the k_6^1-mode. Condon [17] formulated the concept of the rotational strength R_{ba} of an individual electronic absorption band in terms of the product of an electric dipole transition moment and a magnetic dipole transition moment:

$$R_{ba} = \mathrm{Im}\{(a|\boldsymbol{p}|b)(b|\boldsymbol{m}|a)\}. \tag{1}$$

When we disregard the time dependence of $\boldsymbol{m}$, since in InCl we have a static case, we find that $\boldsymbol{\mu} \cdot \boldsymbol{R}$ is a measure of what we call the geometric chirality. Here for $\boldsymbol{\mu}$ we have the choice between $\boldsymbol{\mu}_1$, $\boldsymbol{\mu}_2$ and $\boldsymbol{\mu}_3$. One may check in table 6 that quantities like $\mu_x R_x$ and $\mu_y R_y$ do all add up. Of course, other k_6-vectors exist.

However, a closer look at table 6 shows that $\boldsymbol{Q} \cdot \boldsymbol{F}$ is also a quantity which is induced by the k_6^1-distortion. It is another source of chirality, arising because of the wavelength of the distortion wave being small with respect to the size of the octahedra. The edges of the octahedra are ≈0.35 times the wavelength of the Δ mode. An analogue for $\boldsymbol{Q} \cdot \boldsymbol{F}$ in the theory of optical activity has never been mentioned as far as we are aware. Figure 2 shows pictorially the combination of an electric quadrupole transition moment and a magnetic quadrupole transition moment.

The W waves are formed of circularly transverse waves as well (see table 7). However, neighbouring rows have opposite senses, so the contribution to the overall chirality is zero. On the other hand, these W waves introduce the tetrahedral (A_{2u}) octupoles in yellow InCl.

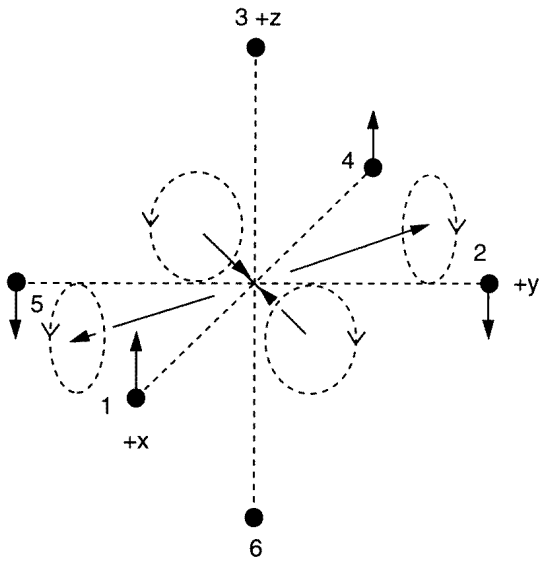

Figure 2. A new type of chirality represented by axial vectors from a dynamic T_{2uz} moment and polar vectors from a T_{2gxy} moment. Note that the senses of the helices are the same for the four quadrants.

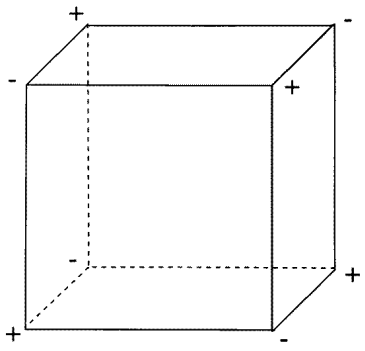

Figure 3. A tetrahedral (A_{2u}) electric octupole.

These are measured by the bilinear expression $\boldsymbol{\mu} \cdot \boldsymbol{Q}$. Therefore the W waves introduce a ferrodistortive tetrahedral electric octupole which belongs to the A_{2u} irrep of point group $m\bar{3}m$ (see figure 3). Another quantity exists, which is formed by $\boldsymbol{R} \cdot \boldsymbol{F}$ and transforms as A_{2u} as well.

Similarly, for the $\boldsymbol{k}_4$-modes one finds the pseudoscalar $\boldsymbol{Q} \cdot \boldsymbol{R}$, which transforms as A_{2g}. Its sum over the unit cell of InCl is, however, zero. With respect to the 'A_{2g}' scalar, the compound with the idealized coordinates is antiferrodistortive. The term $\boldsymbol{\mu} \cdot \boldsymbol{F}$ transforms also as A_{2g}. For the geometric approximation its contribution is exactly zero, however.

Interference occurs between the Δ waves, the W waves and the Σ_4 waves and leads to localization. This can be studied by applying these distortions one after another to rows of ions. This is illustrated here for the simple case of taking only $\boldsymbol{k}_6^1$ (figure 4) and $\boldsymbol{k}_8^1$

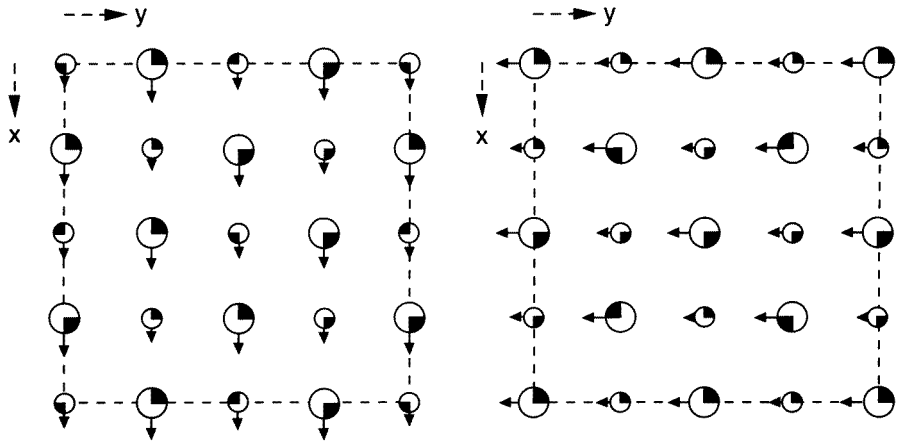

Figure 4. $\boldsymbol{k}_6^1$ for $z = 0$ (left) and $z = 1/4$ (right). In^+ (Cl^-) ions are represented by small (large) circles. The types of ion (1, 2, 3 or 4) are denoted like the quarters of an hour.

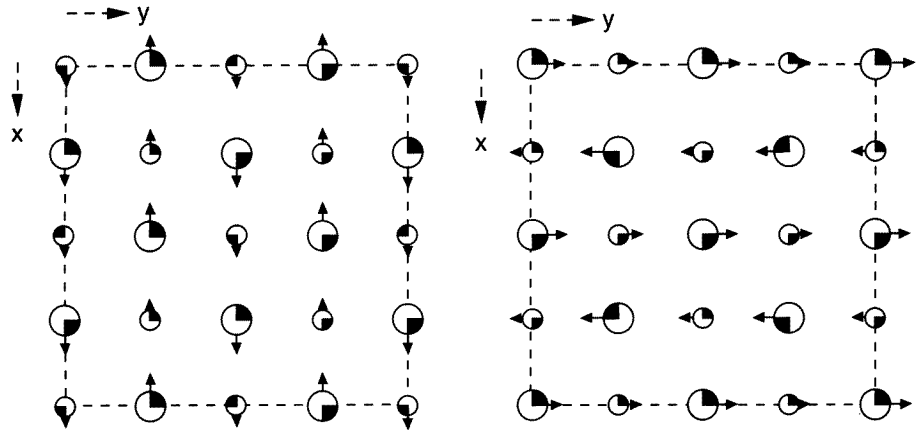

Figure 5. $\boldsymbol{k}_8^1$ for $z = 0$ (left) and $z = 1/4$ (right). The ion notation is the same as that for figure 4.

(figure 5) for the planes at the relative coordinates $z = 0$ and $z = 0.25$. Alternate rows or columns of In and Cl ions show longitudinal shifts, occurring because of the following relations: $w_1 = -d_1; d_2 = -w_2; d_2' = -w_2'; d_1' = w_1'$. In this way, isolated chains are formed which are longitudinally displaced; the distances between anions and cations are alternating.

The complete expressions for the Δ and the W modes (figure 6) show e.g. for $z = 0$ that not only vertically displaced rows exist, but horizontally displaced ones as well. The latter alternate in direction, and it is precisely in between these horizontal lines that the $\boldsymbol{k}_4$-displacements (see figure 7) are situated, so their interaction with the neighbouring lines is in a first approximation zero.

Typical displacement patterns are shown e.g. in figure 7. Along the dotted line all ions in that column experience the same type of even mode, which is shown (figure 11—see later) to consist of a quadrupole component (T_{2g}) and a rotation component (T_{1g}). Similarly,

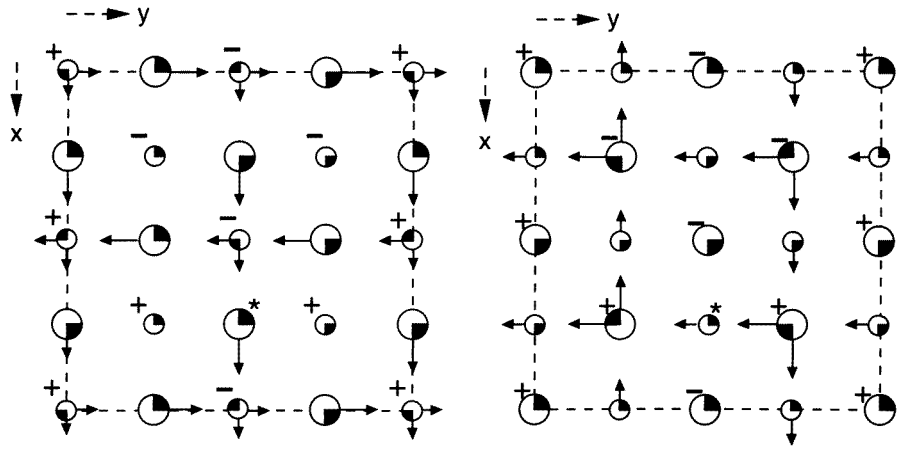

Figure 6. The complete Δ and W modes for $z = 0$ (left) and $z = 1/4$ (right). The asterisk denotes a column of type 1 ions which have parallel T_{2u} modes.

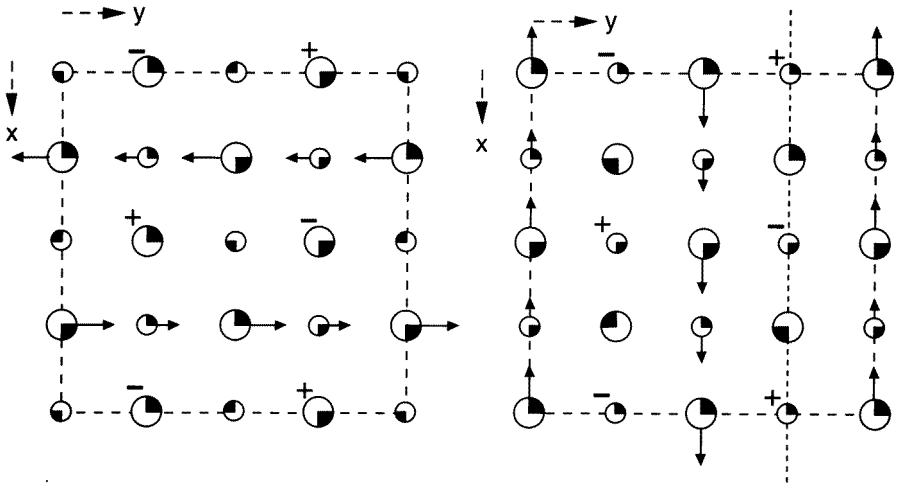

Figure 7. The x-, y-, z-components of the displacements of the Σ_4 modes for $z = 0$ (left) and $z = 1/4$ (right). The dotted line denotes ions with even modes (see figure 11, later).

in all In and Cl ions of type 1 a single T_{2u} component occurs. A column of these ions is denoted with an asterisk in each layer of InCl (figures 8, 9). The typical T_{2u} displacements of the nearest neighbours of these ions are denoted by plus and minus signs. We have tagged these same ions in figure 6 also, which shows that the localization of the T_{2u} modes arises from the combination of Δ and W waves.

Obviously, the longitudinal displacement of rows of ions and the alternation of bonding distances along these rows is characteristic for the distortion from rock salt to yellow InCl. From inspection of figures 4, 5 and 7 it follows that the three different modes show the same characteristic longitudinal pattern. We introduce the longitudinal force constant f and the transverse force constant g for nearest neighbours. It is assumed that these interactions can be described by means of harmonic springs. For the Δ irrep, e.g. $\boldsymbol{e}_1 \cos \boldsymbol{k}_6^1 \cdot \boldsymbol{r}$, the

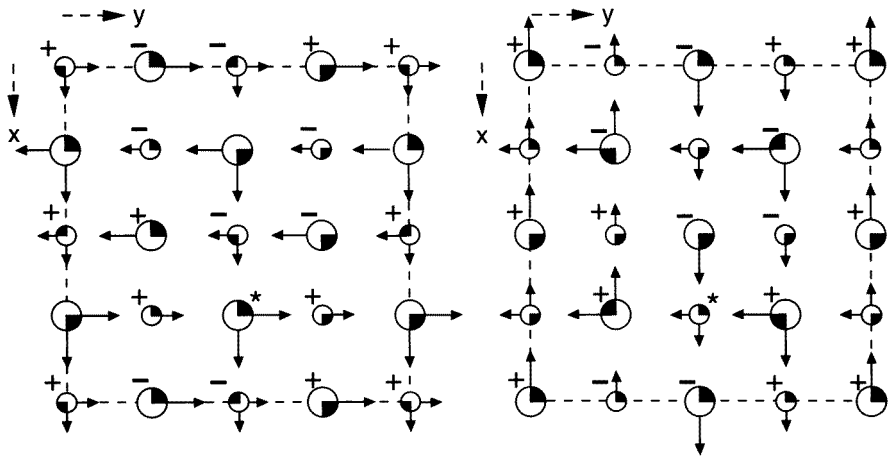

Figure 8. InCl in the 'geometric' approximation; $z = 0$ (left) and $z = \frac{1}{4}$ (right).

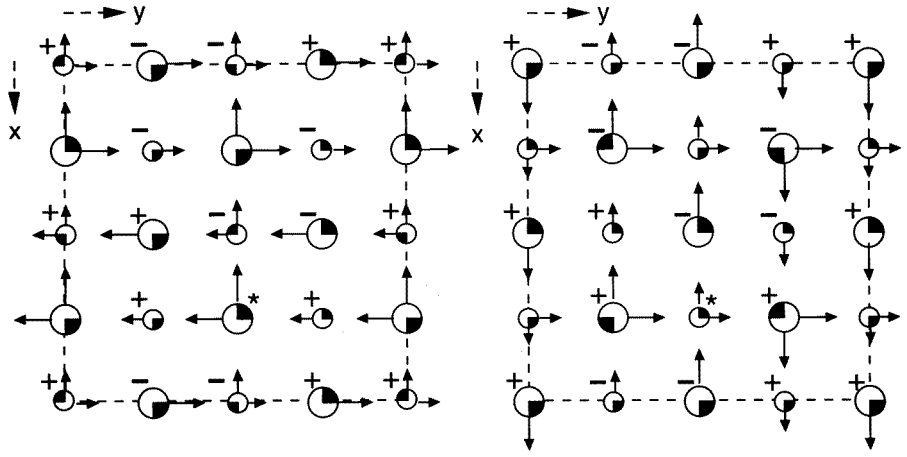

Figure 9. InCl in the 'geometric' approximation; $z = \frac{1}{2}$ (left) $z = \frac{3}{4}$ (right).

energy for one formula unit of an InCl molecule, $E(\Delta)$, is

$$E(\Delta) = f(d_1 - d_1')^2 + g(d_1 - d_1')^2. \tag{2}$$

For the W irrep, e.g. $\boldsymbol{e}_1 \cos \boldsymbol{k}_8^1 \cdot \boldsymbol{r}$,

$$E(\mathrm{W}) = f(w_1 + w_1')^2 + g(w_1 - w_1')^2. \tag{3}$$

Remember that the coordinates w_1 and w_1' differ in sign, which is not the case for d_1 and d_1' or for s_3 and s_3' (see table 4).

Finally, for the Σ_4 irrep, e.g. $\boldsymbol{e}_1 \sin \boldsymbol{k}_4^5 \cdot \boldsymbol{r}$,

$$E(\Sigma_4) = f(s_3 - s_3')^2 + g(s_3^2 + s_3'^2). \tag{4}$$

For this nearest-neighbour interaction and the 'geometric' approximation, we conclude that $E(\Delta)$ is lower in energy by the term $2gd_1d_1'$ than $E(\Sigma_4)$. On the other hand $E(\mathrm{W})$ is higher in energy than $E(\Sigma_4)$ by the same amount. This energy difference is expected to

be small, since $g < f$ and since it looks as if the transverse bonds are broken. Also we assume that the effective mass is equal for the three different modes. In the 'geometric' approximation the Δ and W modes together cause rows of ions to shift. Combined, these two modes are nearly degenerate with the Σ_4 mode. From computer-generated figures (only partly shown in figure 6 and figure 7), we find that for the $\Delta + \mathrm{W}$ case each ion shift has at a distance a_0 a pair of antiparallel- and a pair of parallel-displaced ions. For the Σ_4 modes, however, each ion has at that same distance two pairs of antiparallel-shifted neighbours. We therefore expect the combination of Δ and W waves to be somewhat more stable than the Σ_4 modes.

When the numbers of displaced rows of ions are counted, the Δ irrep and the W irrep contribute together one half of the possible shifts. The Σ_4 irrep contributes a quarter of the possible shifts. This means also that a quarter of the rows have no shift. In figure 8 and figure 9 all shifts in InCl in the 'geometric' approximation are given.

By inspection of the geometry of especially the type 2 $InCl_6$ octahedra, it has been found that in the 'geometric' approximation the symmetry differs considerably from the almost 'trigonal' form. Therefore we think that the driving force required for obtaining the real structure by changing the symmetry coordinates slightly (table 2) is the energetically more favourable shape, with almost point group 3 for the $InCl_6$ octahedra of In type 2 [5].

4. Third-order invariants

Third-order invariants in the sense of Landau's theory for the development of the free energy of the yellow InCl crystal will be derived in this section. For this purpose we refer to tables A4 and A5 (given later, in the appendix), giving the coordinates of representative In and Cl ions. Different sources of anharmonicity exist, and the proportionality constants are not expected to be equal. Let us abbreviate the T_{2g} components to $Q_{\alpha\beta}$, the T_{1u} components to μ_α (the three types have the same group theoretical behaviour), the T_{2u} components to F_α and the T_{1g} components to R_α. This leads to terms of the following type (the cartesian components are given in cyclic order by α, β and γ) (e.g. see the tables given by Watanabe [18]):

$$\chi_q \sum_\alpha Q_{\alpha\beta} \frac{1}{2}\{\mu'_\alpha \mu_\beta + \mu'_\beta \mu_\alpha\} \tag{5}$$

$$\chi_r \sum_\alpha R_\alpha \frac{1}{2}\{\mu'_\beta \mu_\gamma - \mu'_\gamma \mu_\beta\} \tag{6}$$

$$\chi_t \sum_\alpha F_\alpha \{\mu_\beta Q_{\alpha\beta} - \mu_\gamma Q_{\gamma\alpha}\}. \tag{7}$$

The susceptibilities χ_q, χ_r and χ_t have the dimension of energy in our equations, since the three coordinates are expressed as fractions of the cell parameter of the cubic yellow InCl structure. These expressions have to be developed for the In as well as for the Cl sites.

As is usual in the formulation of Landau invariants, they are expressed in terms of the relevant normal coordinates. Results from the tables A4 and A5 (see later, in the appendix), using the geometric approximation and considering table 5, give us for formula (5) for In

$$\frac{32}{3}\sqrt{3}A_{\mathrm{In}}[(d'_1 + w'_1)^2 s_3 + (d'_2 - w'_2)s'_3(d_2 - w_2)] \tag{8}$$

and for Cl

$$\frac{32}{3}\sqrt{3}A_{\mathrm{Cl}}[-(d_2 - w_2)^2 s'_3 - (d_1 - w_1)(d'_1 + w'_1)s_3]. \tag{9}$$

Whereas the third-order terms with quadrupole moments arise from all types of ion, the third-order invariant from equation (6) occurs only for ions of type 2:

$$\frac{8}{3}\sqrt{3}B_{\mathrm{In}}(d_1 - d_2 - w_1 + w_2)[s_3(d_2' - w_2') - (d_1 - w_1)s_3'] \tag{10}$$

$$\frac{8}{3}\sqrt{3}B_{\mathrm{Cl}}(-d_1' + d_2' - w_1' - w_2')[(d_2' - w_2')s_3 - s_3'(d_1 - w_1)]. \tag{11}$$

The strong T_{2u} components for the ions of type 1 give the following invariants (equation (7)):

$$\frac{16}{3}\sqrt{3}C_{\mathrm{In}}(d_1 - d_2 - w_1 + w_2)[s_3'(-d_1 + w_1) + (d_2' - w_2')s_3] \tag{12}$$

$$\frac{16}{3}\sqrt{3}C_{\mathrm{Cl}}(-d_1' + d_2' - w_1' - w_2')[(-d_1 + w_1)s_3' + s_3(d_2' - w_2')]. \tag{13}$$

These invariants have been derived without using the T_{1u2} modes, as this is unnecessary for the discussion.

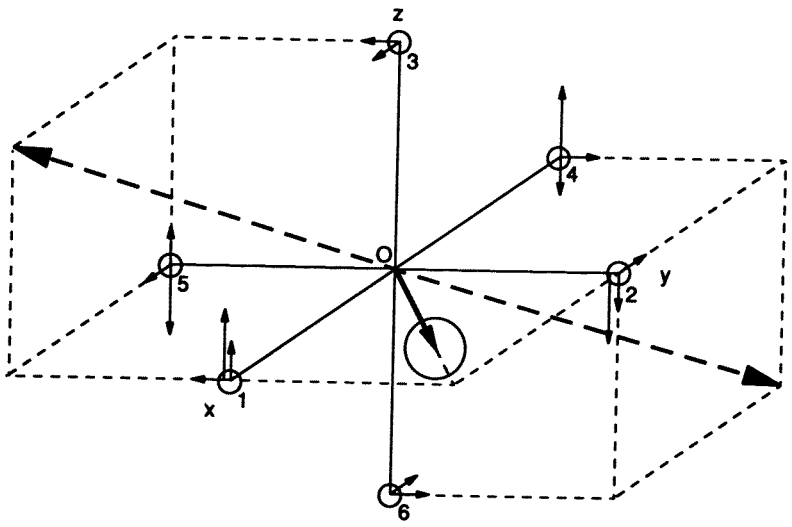

Figure 10. An $In(1)Cl_6$ cluster. In order to distinguish the T_{2u} mode from the others, the lengths of its arrows are shown twice as long.

Whereas it is difficult to say whether equations (5) and (6) contribute much to the energy of the system, the effect of equation (7) seems important. This has been explained by us [5] as the tendency to increase the distance between the Cl ions closest to the lone pair (see figure 10). Suppose that the lone pair is pointing in the [110] direction, between the local positive x-axis and the positive y-axis. The ligands at these axes (numbered 1 and 2) do not give enough room. Their distance can be made longer by increasing the angle between the axes. In addition, the large t_{2uz} coordinate as well as the right combination of the t_{2gzx} and t_{2gzy} coordinates increase the distance between the ligands in the z-direction. Intentionally, the local vectors belonging to the t_{2uz} coordinate are in figure 10 shown twice as long as those belonging to the t_{2g} coordinates. From this picture it is seen that the local scalar products of these coordinates annihilate each other. This has to be so, since the product $T_{2uz}(T_{2gzx} + T_{2gyz})$ is odd for inversion. However, multiplying this by the dipolar

moment directed along [110] changes the relative weight of the positive and the negative contributions, and this results in a third-order term.

The main conclusion of this section is that third-order invariants do indeed exist.

5. Fourth-order invariants

5.1. Ferrodistortive and antiferrodistortive patterns

The symmetry of the point group of the crystal is lowered from $m\bar{3}m$ to 23. It will be shown that for yellow InCl the Δ modes introduce ferrodistortive helical deformations, which transform as the one-dimensional A_{1u} irrep of the point group $m\bar{3}m$ at the Γ point. The W modes introduce tetrahedrons, with deformations transforming as A_{2u} at the Γ point. The Σ_4 modes introduce bilinear quantities transforming as A_{2g}, but at the X point (*vide infra*). Table 8 contains the one-dimensional irreps of the point group $m\bar{3}m$.

Table 8. One-dimensional irreps of the point group $m\bar{3}m$.

$m\bar{3}m$	E	$8C_3$	$6C_2$	$6C_4$	$3C_2$	i	$6S_4$	$8S_6$	$3\sigma_h$	$6\sigma_d$
A_{1g}	1	1	1	1	1	1	1	1	1	1
A_{2g}	1	1	−1	−1	1	1	−1	1	1	−1
A_{1u}	1	1	1	1	1	−1	−1	−1	−1	−1
A_{2u}	1	1	−1	−1	1	−1	1	−1	−1	1

From table 8 it follows that a bilinear quantity transforming as A_{1u} destroys all improper symmetry operations, thus leaving a point group 432 (O). A further reduction in symmetry occurs if a bilinear quantity transforming as A_{2u} is also present. The total reduction results in the group 23 (T), the point group of yellow InCl. The A_{2u} irrep by itself would reduce $m\bar{3}m$ to $\bar{4}3m$ (T_d). The other possibility of a bilinear quantity transforming as the irrep A_{2g} at the Γ point is not realized in this structure.

We will first treat chirality, then tetrahedron formation and finally spiral formation.

5.2. Chirality

The Δ modes appear as transverse planar waves, inducing ferrodistortively ordered static helices in rock salt. It is instructive to consider these planar waves first in view of the analogy with the familiar phenomenon of optical rotatory power.

The bilinear quantity which in a cubic system transforms as A_{1u} takes the form $xR_x + yR_y$ for a circular standing wave along the z-direction. Here x and y are the transverse displacements, and R_x and R_y are rotation components.

$\boldsymbol{\mu} \cdot \boldsymbol{R}$ may be expressed also in terms of the following rotational strength for static helices along the z-axis (see Maaskant and Haije [19]):

$$\mathrm{Gyr} = \sum_n P_{x,n}[P_{y,(n+1)} - P_{y,(n-1)}]/a_0 - P_{y,n}[P_{x,(n+1)} - P_{x,(n-1)}]/a_0. \quad (14)$$

This equation is essentially $\boldsymbol{P} \cdot \boldsymbol{\nabla} \times \boldsymbol{P}$, where $\boldsymbol{P}$ denotes a shift of ions. In this paper differentials are replaced by differences, and n numbers the planes perpendicular to the z-axis. Only combinations of In^+ and Cl^- ions are considered. Gyr, however, will be treated as a geometric object. It will not be necessary to introduce charges. We include a

normalization constant:

$$\mathrm{Gyr}(\boldsymbol{k}_6^1) = \frac{2}{3a_0N}\sum_n \left[d_1'd_2(1+\cos 2\boldsymbol{k}_6^1\cdot\boldsymbol{r}) + d_2'd_1(1-\cos 2\boldsymbol{k}_6^1\cdot\boldsymbol{r})\right] \tag{15}$$

Since for the idealized situation $d_1'd_2 = d_2'd_1$ the cosines annihilate each other. The result for the three directions is

$$\mathrm{Gyr}(\Delta) = \frac{2}{a_0}[d_1'd_2 + d_2'd_1]. \tag{16}$$

$\mathrm{Gyr}(\Delta)$ transforms as A_{1u}, $\boldsymbol{k} = 0$, and describes the ferrodistortive ordering of static helices along the three directions of the cell axes. Note that $\boldsymbol{\mu}\cdot\boldsymbol{R}$ as well as $\boldsymbol{Q}\cdot\boldsymbol{F}$ are included in equation (16). This follows from table 6, where both quantities occur under the action of one of the Δ modes. The square of $\mathrm{Gyr}(\Delta)$ is a correct Landau fourth-order invariant.

The W irreps do not induce ferrodistortive chirality. Because of the special positions of the cations and anions, the displacements show helices of alternating sense arranged along the cell axes. This can be proven by applying equation (14) for example to $\boldsymbol{k}_8^1$:

$$\mathrm{Gyr}(\boldsymbol{k}_8^1) = \frac{2}{3a_0N}\sum_n \left[w_1'w_2(1+\cos 2\boldsymbol{k}_8^1) + w_2'w_1(1-\cos 2\boldsymbol{k}_8^1)\right]. \tag{17}$$

For the ideal case $w_2'w_1 = -w_1'w_2$. Therefore, the result for the W modes is

$$\mathrm{Gyr}(W) = \frac{2}{3a_0}[w_1'w_2 - w_2'w_1][\cos 2\boldsymbol{k}_8^1\cdot\boldsymbol{r} + \cos 2\boldsymbol{k}_8^2\cdot\boldsymbol{r} + \cos 2\boldsymbol{k}_8^3\cdot\boldsymbol{r}]. \tag{18}$$

This represents antiferrodistortively ordered chirality belonging to the X point in the first B.Z.. Since for the fcc lattice $2\boldsymbol{k}_8^1$ is equivalent to $2\boldsymbol{k}_6^1$ and similarly for the other components, equation (18) corresponds to an $\mathcal{A}_3$ distribution (equation (A3)).

The Σ_4 waves also cause antiferrodistortively ordered chirality, but with the $\mathcal{A}_2$ distribution (equation (A2)):

$$\begin{aligned}\mathrm{Gyr}(\Sigma) = -\frac{1}{a_0}s_3s_3'[&\sin\boldsymbol{k}_4^1\cdot\boldsymbol{r} + \sin\boldsymbol{k}_4^2\cdot\boldsymbol{r} + \sin\boldsymbol{k}_4^5\cdot\boldsymbol{r}\\ &+ \sin\boldsymbol{k}_4^6\cdot\boldsymbol{r} + \sin\boldsymbol{k}_4^9\cdot\boldsymbol{r} + \sin\boldsymbol{k}_4^{10}\cdot\boldsymbol{r}].\end{aligned} \tag{19}$$

We have studied the chirality on the computer, for waves propagating along the z-axis of the three types of wave vector: $\boldsymbol{k}_6^1$, $\boldsymbol{k}_8^1$ and those $\boldsymbol{k}_4$-vectors which have only distortions along the $\boldsymbol{e}_1$- and $\boldsymbol{e}_2$-axes. The $\boldsymbol{k}_6^1$-vector alone gives completely delocalized waves. However, as soon as the other waves are added, localization occurs, such that the chiral effect is localized in rows of alternating cations and anions of type 1. We next studied the behaviour of the T_{2u} moments, which occur in the scalar product $\boldsymbol{F}\cdot\boldsymbol{Q}$. These moments are formed by Δ and W modes. Again interference is noted. On applying all $\boldsymbol{k}_6$- and $\boldsymbol{k}_8$-vectors, only one strong component remains for the cations and anions of type 1.

The chirality due to the Δ waves is not only ferrodistortive, but their combination induces a term of $\mathcal{A}_2$-type (equation (A2)) as well. A similar term arises from the combination of W modes, which induce the tetrahedron character (equation (22)). A nice example of such an antiferrodistortive arrangement arising through the interaction of waves of different origin is that In(3) and In(4) octahedra differ in sign as regards the chirality as well as the tetrahedron character. This can only be true by means of the $\mathcal{A}_4$ scalar which belongs to the L point (see equation (A4)), arising from the product of Σ_4 and Δ and/or W modes. This can be shown from tables A4 and A5—see later.

5.3. Tetrahedral distortion from the cube

By analogy with equation (14),

$$\text{Tetr} = \sum_n P_{x,n}[P_{y,(n+1)} - P_{y,(n-1)}]/a_0 + P_{y,n}[P_{x,(n+1)} - P_{x,(n-1)}]/a_0. \tag{20}$$

This equation differs from equation (14) in having a + sign in the middle. It transforms as xyz and leads to correct results. For the $\boldsymbol{k}_8^1$-mode for instance, it is found that

$$\text{Tetr}(\boldsymbol{k}_8^1) = \frac{2}{3a_0N}\sum_n \left[w_1'w_2(1+\cos 2\boldsymbol{k}_8^1\cdot\boldsymbol{r}) - w_2'w_1(1-\cos 2\boldsymbol{k}_8^1\cdot\boldsymbol{r})\right] \tag{21}$$

which gives for the complete W waves

$$\text{Tetr(W)} = \frac{2}{a_0}(w_1'w_2 - w_2'w_1). \tag{22}$$

Like Gyr(Δ), Tetr(W) arises from two sources: $\boldsymbol{\mu}\cdot\boldsymbol{Q}$ and $\boldsymbol{R}\cdot\boldsymbol{F}$ (see table 7).

The Δ waves and the Σ_4 waves lead to antiferrodistortive arrangements:

$$\text{Tetr}(\Delta) = \frac{2}{3}\frac{1}{a_0}(d_1'd_2 + d_2'd_1)(\cos 2\boldsymbol{k}_6^1\cdot\boldsymbol{r} + \cos 2\boldsymbol{k}_6^2\cdot\boldsymbol{r} + \cos 2\boldsymbol{k}_6^3\cdot\boldsymbol{r}) \tag{23}$$

$$\begin{aligned}\text{Tetr}(\Sigma) = \frac{1}{a_0}s_3s_3'[&\sin\boldsymbol{k}_4^1\cdot\boldsymbol{r} + \sin\boldsymbol{k}_4^2\cdot\boldsymbol{r} + \sin\boldsymbol{k}_4^5\cdot\boldsymbol{r}\\ &+ \sin\boldsymbol{k}_4^6\cdot\boldsymbol{r} + \sin\boldsymbol{k}_4^9\cdot\boldsymbol{r} + \sin\boldsymbol{k}_4^{10}\cdot\boldsymbol{r}].\end{aligned} \tag{24}$$

5.4. Spiral formation

There is another bilinear quantity that is unknown as far as we are aware, and is induced by the Σ_4 modes. Characteristic of this are distortions shaped as one half of a swastika (see figure 11). It is as if twinning occurs as a result of shearing—however, without leading to domain formation. We named this type of deformation a spiral, because of the similarity of its shape to a watch spring or a spiral galaxy. Spirals transform as A_{2g}, but only antiferrodistortive ordering is found in the structure of InCl. The bilinear form is a product of the expressions for the rotations and quadrupoles to be expected for the $\boldsymbol{k}_4$-modes.

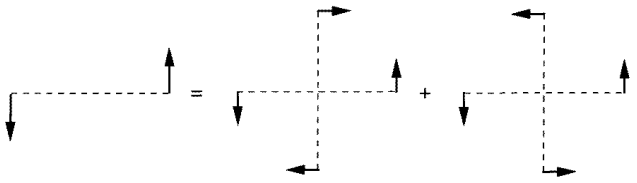

Figure 11. The decomposition of an even mode into a quadrupole (T_{2g}) and a rotation (T_{1g}). Their product represents a part of the bilinear pseudoscalar which transforms as A_{2g}.

There are two expressions belonging to irrep $\tau_4(B_2)$ also, such as that for the Σ_4 normal mode (see table A1 later). These are

$$\begin{aligned}[&\{(Q_{yz}+Q_{zx})/\sqrt{2}\}\cos\boldsymbol{k}_4^1\cdot\boldsymbol{r} + \{(Q_{yz}-Q_{zx})/\sqrt{2}\}\cos\boldsymbol{k}_4^2\cdot\boldsymbol{r}\\ &+ \{(Q_{zx}+Q_{xy})/\sqrt{2}\}\cos\boldsymbol{k}_4^5\cdot\boldsymbol{r} + \{(Q_{zx}-Q_{xy})/\sqrt{2}\}\cos\boldsymbol{k}_4^6\cdot\boldsymbol{r}\\ &+ \{(Q_{xy}+Q_{yz})/\sqrt{2}\}\cos\boldsymbol{k}_4^9\cdot\boldsymbol{r} + \{(Q_{xy}-Q_{yz})/\sqrt{2}\}\cos\boldsymbol{k}_4^{10}\cdot\boldsymbol{r}]\end{aligned} \tag{25}$$

$$[\{(R_x - R_y)/\sqrt{2}\}\cos \boldsymbol{k}_4^1 \cdot \boldsymbol{r} + \{(R_x + R_y)/\sqrt{2}\}\cos \boldsymbol{k}_4^2 \cdot \boldsymbol{r} + \{(R_y - R_z)/\sqrt{2}\}\cos \boldsymbol{k}_4^5 \cdot \boldsymbol{r} + \{(R_y + R_z)/\sqrt{2}\}\cos \boldsymbol{k}_4^6 \cdot \boldsymbol{r} + \{(R_z - R_x)/\sqrt{2}\}\cos \boldsymbol{k}_4^9 \cdot \boldsymbol{r} + \{(R_z + R_x)/\sqrt{2}\}\cos \boldsymbol{k}_4^{10} \cdot \boldsymbol{r}]. \quad (26)$$

The distributions of the quadrupoles, according to equation (25), and of the rotations (equation (26)) have been checked by a computer program.

Multiplying these expressions gives

$$J = R_x Q_{yz}[\cos 2\boldsymbol{k}_6^1 \cdot \boldsymbol{r} + \cos 2\boldsymbol{k}_6^3 \cdot \boldsymbol{r}] + R_y Q_{zx}[\cos 2\boldsymbol{k}_6^2 \cdot \boldsymbol{r} + \cos 2\boldsymbol{k}_6^3 \cdot \boldsymbol{r}] + R_z Q_{xy}[\cos 2\boldsymbol{k}_6^1 \cdot \boldsymbol{r} + \cos 2\boldsymbol{k}_6^2 \cdot \boldsymbol{r}]. \quad (27)$$

This expression clearly belongs to the X point. Although individually the Δ and the W modes build up a distribution like J, these compensate each other in the idealized crystal. Therefore, only the Σ modes contribute:

$$\mathrm{Spir}(\Sigma_4) = [c_1 s_3^2 + c_2 s_3'^2]J. \quad (28)$$

This results in unusual antiferrodistortive ordering of the type A_{2g}, with, for the In ions, $-s_3^2$, $-s_3^2$, $3s_3^2$ and $3s_3^2$ for the first to the fourth type respectively, and $s_3'^2$, $s_3'^2$, $-3s_3'^2$ and $-3s_3'^2$ for the Cl ions of the first to the fourth type, respectively.

5.5. Final forms

Expressing the fourth-order Landau invariants as a function of their d-, w- and s-amplitudes is very complex, since through interference terms they reinforce or annihilate each other. The easiest way of describing the important Landau invariants is to work with table 5. When the explicit formulae in terms of the algebraic amplitudes are required, use can be made of the tables A4 and A5—see later.

The most important second-order invariant is probably the interaction between the shifts of the ions with respect to their immediate neighbours. This is through the scalar product of $\boldsymbol{q}(t_{1u1}) \cdot \boldsymbol{q}(t_{1u2})$. From table 5 one sees directly that the T_{1u1} and the T_{1u2} coordinates are collinear. The type 1 and 2 ions contribute only two thirds as much as the type 3 and 4 ions, which corresponds to the digonal and trigonal character of these octahedra, respectively. It corresponds also to the longitudinal distortions of the lines of ions.

Other second-order invariants are formed from A_{1g} products of the following three-component moments with themselves: the rotations or the quadrupoles, or the three types of T_{1u} and T_{2u} moment. All of these second-order invariants lead to fourth-order invariants also.

On forming scalar products of the T_{1g} and, for example, the T_{1u1}, A_{1u} products are obtained, which have values in proportion to 2, 0, -3, 3 for the four types of In ion, and 2, 0, 3, -3 for the four types of Cl ion. We have to include in addition for the type 1 ions the T_{2u} component, which together with the corresponding T_{2g} component, contributes to the A_{1u} scalar. The type 2 ions also contribute to this type of scalar through the product of $\boldsymbol{q}(t_{1u3})$ and $\boldsymbol{q}(t_{1g})$ only.

We can form A_{2u} scalars by combining T_{2g} with for example, T_{1u1}. They contribute in proportion to 0, 2, -3, 3 for the In ions and 0, -2, -3, 3 for the Cl ions. However, the $q(t_{1u3z}) \times q(t_{2gxy})$-term for In(2) and the corresponding term for Cl(2) should also be included. One should also include the $q(t_{2uz})$-term for In(1), which, multiplied with $q(t_{1gz})$, also contributes to this A_{2u} scalar.

The A_{2g} pseudoscalars are formed by multiplying $\boldsymbol{q}(t_{1g})$ and $\boldsymbol{q}(t_{2g})$. For the In sublattices 1–4 these are in the proportion -1, -1, 3, 3 and for Cl they are in the proportion 1, 1, -3, -3 respectively.

There are therefore fourth-order invariants of different parentage: those derived from the A_{1g}, A_{1u}, A_{2u} and A_{2g} scalars.

6. Discussion

In the Landau theory of second-order phase transitions [14, 15] one studies the possibility of a development of the thermodynamic potential (usually called the free energy) in a power series of the so-called order parameter. When the so-called Landau conditions (LC) are fulfilled, a second-order phase transition occurs at the temperature where the coefficient of the harmonic term is zero. This Landau theory describes many second-order phase transitions. But in addition the development is possible for a number of phase transitions which do not fulfil the Landau conditions (see, e.g., [20, 21]).

We imagine the following hypothetical phase transition. Let the shifts of the rows of ions be denoted by the order parameter η, and let the ratio between the In and the Cl shifts remain constant. Then the development becomes

$$F = F_0 + A\eta^2 + B\eta^3 + C\eta^4 + \cdots. \tag{29}$$

Here F_0 is the free energy of the high-symmetry phase. In general, for just a distortion belonging to a single irrep, the A-constant varies from positive ($T > T_c$) towards zero (at T_c). At $T = T_c$ a continuous phase transition sets in, provided that four Landau conditions are fulfilled.

We now discuss these conditions, recapitulating the different grounds which support our view.

LC1. The new structure should have a space group, which is a subgroup of the high-symmetry space group of the parent structure.

The experimental proof of the rock-salt structure being the appropriate parent structure in this case is supported by the following facts:

(a) from the three-dimensional Patterson function a deformed rock-salt structure was established [1–3];

(b) AB compounds with cations with a similar outer electronic configurations (from the so-called p-block elements) occur often either with the rock-salt structure or a deformed rock-salt structure [6];

(c) red InCl with the β-TlI structure shows double layers with the rock-salt stacking [12, 13]; and

(d) the relationship between the yellow InCl structure and the rock-salt structure is clearly demonstrated in table 1.

LC2. Only a lattice mode belonging to *one* irreducible representation is allowed for a second-order transition.

We found three equally strong normal coordinates belonging to different irreps and that are pseudo-degenerate. In our opinion the treatment of this hypothetical phase transition should be started taking into account these three modes, *vide infra*.

LC3. A third-order term should not be present [15, 20]. Or, to express this differently, the constant B (equation (29)) should be zero by symmetry. In section 4 we have given evidence that such a third-order term is present. It consists of products of the three main irreps. This means that the hypothetical phase transition is of first order.

LC4. This condition is also called the Lifshitz condition. The structure should be stable for small variations of the wave vector. Antisymmetric squares of the actual irrep should

not contain a part which transforms as a vector component [15]. Haas [22] gave a different proof, which can be expressed by the requirement that the proper symmetry group of $\boldsymbol{k}$ has no invariant vectors. The W irreps (the group of $\boldsymbol{k}$ is D_{2d}) fulfil LC4, but the Δ and the Σ_4 modes (the groups of $\boldsymbol{k}$ are C_{4v} and C_{2v}, respectively) do not fulfil LC4. However, the third-order term couples these waves and probably the W modes also fix the others. No sign of an incommensurate phase has been found, experimentally.

A further condition for a second-order phase transition is that the constant C in equation (29) should be positive in order to keep η bounded. In the case where C is negative, powers higher than four have to be studied in order to prevent $|\eta|$ from increasing to infinity.

The case of LC2 needs closer inspection. Let us for the moment consider the case in which three different lattice modes have exactly the same eigenfrequencies. The deformed structure then has to be a superposition of these three modes. Physically, one would expect such a structure to have a certain tolerance for deviating conditions. One expects such a structure to remain essentially the same for a not too large mode of another irrep, or when the eigenfrequencies of the large modes are not exactly equal. In our opinion this is the case for yellow InCl.

This means that here the second Landau condition does not apply. Landau also had a different experiment in mind. He imagined a continuous change in temperature with nearly infinite precision, which could discriminate between the A-constants (equation (29)) of the three relevant modes. In our case, however, a phase transition has not been found. In addition, from LC3, it would be of first order.

The description of this hypothetical phase transition as a successive series of phase transitions failed, because of a lack of experimental evidence. Also, treating one of the three relevant modes as a starting point has no experimental support.

We treated the strong modes in an equivalent way, with equal (absolute) amplitudes. This has been called the 'geometric' approximation. Table 4 shows that the remaining differences from the experiment are an order of magnitude smaller than the deviations from the rock-salt structure. Therefore, we believe that we have understood the essence of the structure of yellow InCl. The picture of the cooperative distortion in InCl is best given by figures 8 and 9. The real structure differs only slightly, the space group remaining the same.

The desired picture of the cooperative distortion is given by our 'geometric' approximation. The essence of it is that the deformation consists of longitudinal displacements of rows of ions, with different shifts for the anions and the cations. This kind of displacement, where the rows seem to act independently, is produced by modes of the Δ, W and Σ_4 type. That the force constants of these modes are nearly equal is intuitively clear from the rock-salt structure. We have here a case of supersymmetry.

The idealized structure of the 'geometric' approximation also allows us to explicitly describe the introduction of chirality, tetrahedral character and spiral distributions. From table 4 it follows that this approximation does indeed treat the main distortion. The change thereafter is most probably caused by the octahedra around the In(2) ions, which 'prefer' a more trigonal distortion [5]. So the real structure consists of 12 digonally and 20 trigonally distorted octahedra. This case of deformed octahedra of mixed kinds is probably stabilized through the cooperative interactions. This coexistence of differently distorted octahedra occurs more often in solid-state compounds. For example hexagonal $BaTiO_3$ and $BaMnO_3$ have crystal structures with mixed hexagonal/cubic packings [23].

The complexity of this InCl structure arises because, for a good representation, the trigonally distorted octahedra demand threefold axes of quantization, whereas for the digonal

octahedra of type 1, fourfold axes are more appropriate (see figure 1). A further increase of complexity is due to the many different moments which coexist (table 5). We have seen a similar situation, but slightly simpler, for $CsCuCl_3$ [19], where even and odd moments coexist. These occur for yellow InCl, since one has to consider little groups of rather low order ($4mm$, $\bar{4}2m$ and $2mm$) for respectively the Δ, W and Σ_4 modes. Especially interesting is the occurrence of electrical octupoles (T_{2u}).

The reduction of the point group of the crystal has been studied in order to identify bilinear pseudoscalars. This method is new, as far as we are aware. We found ferrodistortive as well as antiferrodistortive distributions of chirality and tetrahedral distortion. We introduced the concept of geometric chirality and found contributions from the octupoles, for which optical counterparts have never been observed. This goes beyond the Condon approximation [17] and arises for yellow InCl because the wavelength of the distortions is $\approx$three times the edge length of an octahedron.

The tetrahedron formation can easily be envisaged. All $InCl_6$ octahedra, except those of type 1, have (approximately) $3m$ symmetry for which locally xyz is an invariant. The dipolar axes lie along one of the body diagonals (eight directions). Since there are 20 octahedra of this type, the cubic structure has to be broken. However, 20 octahedra can form a tetrahedral structure and this is what actually occurs. The digonal octahedra (of type 1) have their dipolar moments along one of the [110] axes or equivalent directions, i.e. just in between two neighbouring corners of a cube.

Also interesting is the interference which occurs between the different normal modes. This leads to localization at the different sites. For example, the In(1) and Cl(1) ions lie on lines, and the geometric chirality is concentrated on them. The In(2) and Cl(2) ions also lie on lines and bear tetrahedral distortions. The ions of types 3 and 4 show chirality as well as tetrahedron formation. Only in the geometric approximation do the type 3 and type 4 ions form exactly each other's opposites.

The effect of just the Σ_4 modes leading to the S.G. $Pa\bar{3}$ (T_h^6) is new. $Pa\bar{3}$ contains inversion; it is a supergroup of $P2_13$ with index 2. Characteristic of this group are the even distortions, called spirals, which consist of a superposition of a rotation (T_{1g}) and a quadrupole (T_{2g}). These form a bilinear scalar product of the A_{2g} type with antiferrodistortive ordering of a new kind. The values for the In(3) and In(4) sites are three times the values for the In(1) and In(2) sites, and of the opposite sign.

Appendix A

A.1. Lattice deformation coordinates

In this subsection the deformations of the rock-salt structure will be evaluated in symmetry modes of the space group $Fm\bar{3}m$. The unit cell of InCl is primitive cubic with a cell parameter of $2a_0$, where a_0 is the cell parameter of the cubic cell ($Z = 4$) of a rock-salt-type structure. In addition we will give the local octahedron modes.

The space group $P2_13$ [24] contains group elements such as zxy and yzx (in the Jones faithful representation; see, e.g., [25]), which are rotations of $2\pi/3$ around (111), and rotations of π along the cell axes, with extra translations. We use the notation of Kovalev [26] where $h_2 = x\bar{y}\bar{z}, h_3 = \bar{x}y\bar{z}$ and $h_4 = \bar{x}\bar{y}z$. The translations are in units of a_0. The space group elements for the last three are then: $\{h_2|1, 1, 0\}, \{h_3|0, 1, 1\}, \{h_4|1, 0, 1\}$.

We have to study expressions such as $\boldsymbol{e}_1 \exp \mathrm{i}\boldsymbol{k}_s^m \cdot \boldsymbol{r}$, identifying those that are invariant for the group elements of $P2_13$. Here $\boldsymbol{e}_1, \boldsymbol{e}_2$ and $\boldsymbol{e}_3$ are unit vectors along respectively

Table A1. Normalized symmetry modes of the ion shifts in InCl for the space group $Fm\bar{3}m$.

c_i		$G(\boldsymbol{k})$	τ_i
d_1	$\sqrt{2/3N}\{\boldsymbol{e}_1\cos\boldsymbol{k}_6^1\cdot\boldsymbol{r}+\boldsymbol{e}_3\cos\boldsymbol{k}_6^2\cdot\boldsymbol{r}+\boldsymbol{e}_2\cos\boldsymbol{k}_6^3\cdot\boldsymbol{r}\}$	T119($4mm$)	τ_5(E)
d_2	$\sqrt{2/3N}\{\boldsymbol{e}_2\sin\boldsymbol{k}_6^1\cdot\boldsymbol{r}+\boldsymbol{e}_1\sin\boldsymbol{k}_6^2\cdot\boldsymbol{r}+\boldsymbol{e}_3\sin\boldsymbol{k}_6^3\cdot\boldsymbol{r}\}$	T119($4mm$)	τ_5(E)
w_1	$\sqrt{2/3N}\{\boldsymbol{e}_1\cos\boldsymbol{k}_8^1\cdot\boldsymbol{r}+\boldsymbol{e}_3\cos\boldsymbol{k}_8^2\cdot\boldsymbol{r}+\boldsymbol{e}_2\cos\boldsymbol{k}_8^3\cdot\boldsymbol{r}\}$	T131($\bar{4}2m$)	τ_5(E)
w_2	$\sqrt{2/3N}\{\boldsymbol{e}_2\sin\boldsymbol{k}_8^1\cdot\boldsymbol{r}+\boldsymbol{e}_1\sin\boldsymbol{k}_8^2\cdot\boldsymbol{r}+\boldsymbol{e}_3\sin\boldsymbol{k}_8^3\cdot\boldsymbol{r}\}$	T131($\bar{4}2m$)	τ_5(E)
s_1	$\sqrt{1/6N}\{(\boldsymbol{e}_1+\boldsymbol{e}_2)\cos\boldsymbol{k}_4^1\cdot\boldsymbol{r}+(\boldsymbol{e}_2+\boldsymbol{e}_3)\cos\boldsymbol{k}_4^5\cdot\boldsymbol{r}+(\boldsymbol{e}_3+\boldsymbol{e}_1)\cos\boldsymbol{k}_4^9\cdot\boldsymbol{r}$		
	$+(\boldsymbol{e}_1-\boldsymbol{e}_2)\cos\boldsymbol{k}_4^2\cdot\boldsymbol{r}+(\boldsymbol{e}_2-\boldsymbol{e}_3)\cos\boldsymbol{k}_4^6\cdot\boldsymbol{r}+(\boldsymbol{e}_3-\boldsymbol{e}_1)\cos\boldsymbol{k}_4^{10}\cdot\boldsymbol{r}\}$	T146($2mm$)	$\tau_1(\mathrm{A}_1)$
s_2	$\sqrt{1/6N}\{(\boldsymbol{e}_1-\boldsymbol{e}_2)\cos\boldsymbol{k}_4^1\cdot\boldsymbol{r}+(\boldsymbol{e}_2-\boldsymbol{e}_3)\cos\boldsymbol{k}_4^5\cdot\boldsymbol{r}+(\boldsymbol{e}_3-\boldsymbol{e}_1)\cos\boldsymbol{k}_4^9\cdot\boldsymbol{r}$		
	$+(\boldsymbol{e}_1+\boldsymbol{e}_2)\cos\boldsymbol{k}_4^2\cdot\boldsymbol{r}+(\boldsymbol{e}_2+\boldsymbol{e}_3)\cos\boldsymbol{k}_4^6\cdot\boldsymbol{r}+(\boldsymbol{e}_3+\boldsymbol{e}_1)\cos\boldsymbol{k}_4^{10}\cdot\boldsymbol{r}\}$	T146($2mm$)	$\tau_3(\mathrm{B}_1)$
s_3	$\sqrt{1/3N}\{+\boldsymbol{e}_3\sin\boldsymbol{k}_4^1\cdot\boldsymbol{r}+\boldsymbol{e}_1\sin\boldsymbol{k}_4^5\cdot\boldsymbol{r}+\boldsymbol{e}_2\sin\boldsymbol{k}_4^9\cdot\boldsymbol{r}$		
	$-\boldsymbol{e}_3\sin\boldsymbol{k}_4^2\cdot\boldsymbol{r}-\boldsymbol{e}_1\sin\boldsymbol{k}_4^6\cdot\boldsymbol{r}-\boldsymbol{e}_2\sin\boldsymbol{k}_4^{10}\cdot\boldsymbol{r}\}$	T146($2mm$)	$\tau_4(\mathrm{B}_2)$
l_1	$\sqrt{1/6N}\{(\boldsymbol{e}_1+\boldsymbol{e}_2+\boldsymbol{e}_3)\cos\boldsymbol{k}_9^1\cdot\boldsymbol{r}+(\boldsymbol{e}_1-\boldsymbol{e}_2-\boldsymbol{e}_3)\cos\boldsymbol{k}_9^2\cdot\boldsymbol{r}$		
	$+(-\boldsymbol{e}_1+\boldsymbol{e}_2-\boldsymbol{e}_3)\cos\boldsymbol{k}_9^3\cdot\boldsymbol{r}+(-\boldsymbol{e}_1-\boldsymbol{e}_2+\boldsymbol{e}_3)\cos\boldsymbol{k}_9^4\cdot\boldsymbol{r}\}$	T221($\bar{3}m$)	$\tau_4(\mathrm{A}_{2\mathrm{u}})$
l_2	$\sqrt{1/6N}\{(\boldsymbol{e}_1+\boldsymbol{e}_2+\boldsymbol{e}_3)\sin\boldsymbol{k}_9^1\cdot\boldsymbol{r}+(\boldsymbol{e}_1-\boldsymbol{e}_2-\boldsymbol{e}_3)\sin\boldsymbol{k}_9^2\cdot\boldsymbol{r}$		
	$+(-\boldsymbol{e}_1+\boldsymbol{e}_2-\boldsymbol{e}_3)\sin\boldsymbol{k}_9^3\cdot\boldsymbol{r}+(-\boldsymbol{e}_1-\boldsymbol{e}_2+\boldsymbol{e}_3)\sin\boldsymbol{k}_9^4\cdot\boldsymbol{r}\}$	T221($\bar{3}m$)	$\tau_4(\mathrm{A}_{2\mathrm{u}})$

the a-, b- and c-axes of the unit cell of InCl. The $\boldsymbol{k}_s^m$ are vectors in the reciprocal cell of $Fm\bar{3}m$. s labels the star (the notation is that of Kovalev [26]) ($4=\Sigma$, $6=\Delta$, $8=\mathrm{W}$, $9=\mathrm{L}$). m labels the members of the star. For example, $\boldsymbol{e}_3\exp\mathrm{i}\boldsymbol{k}_6^1\cdot\boldsymbol{r}$ is not invariant for all group elements. The expression changes sign for $\{h_4|1,0,1\}$. On the other hand $\{h_2|1,1,0\}\boldsymbol{e}_1\exp\mathrm{i}\boldsymbol{k}_6^1\cdot\boldsymbol{r}=\boldsymbol{e}_1\exp\mathrm{i}\boldsymbol{k}_6^1\cdot\boldsymbol{r}$. Also $\{h_3|0,1,1\}\boldsymbol{e}_1\exp\mathrm{i}\boldsymbol{k}_6^1\cdot\boldsymbol{r}=\boldsymbol{e}_1\exp-\mathrm{i}\boldsymbol{k}_6^1\cdot\boldsymbol{r}$, and $\{h_4|1,0,1\}\boldsymbol{e}_1\exp\mathrm{i}\boldsymbol{k}_6^1\cdot\boldsymbol{r}=\boldsymbol{e}_1\exp\mathrm{i}\boldsymbol{k}_6^1\cdot\boldsymbol{r}$. Therefore $\boldsymbol{e}_1\cos\boldsymbol{k}_6^1\cdot\boldsymbol{r}$ is invariant for the three π-rotations. Applying the rotations by $2\pi/3$ around [111] gives the first row of table A1. The other expressions are derived in a similar way.

Table A2. $\boldsymbol{k}$-vector definitions of the different stars.

$\boldsymbol{k}_6^1=-\boldsymbol{k}_6^4=\pi(0,0,1)/a_0$	$\boldsymbol{k}_8^1=-\boldsymbol{k}_8^4=\pi(2,0,1)/a_0$	$\boldsymbol{k}_4^1=\pi(1,1,0)/a_0$	$\boldsymbol{k}_4^2=\pi(1,\bar{1},0)/a_0$
$\boldsymbol{k}_6^2=-\boldsymbol{k}_6^5=\pi(0,1,0)/a_0$	$\boldsymbol{k}_8^2=-\boldsymbol{k}_8^5=\pi(0,1,2)/a_0$	$\boldsymbol{k}_4^5=\pi(0,1,1)/a_0$	$\boldsymbol{k}_4^6=\pi(0,1,\bar{1})/a_0$
$\boldsymbol{k}_6^3=-\boldsymbol{k}_6^6=\pi(1,0,0)/a_0$	$\boldsymbol{k}_8^3=-\boldsymbol{k}_8^6=\pi(1,2,0)/a_0$	$\boldsymbol{k}_4^9=\pi(1,0,1)/a_0$	$\boldsymbol{k}_4^{10}=\pi(\bar{1},0,1)/a_0$
$\boldsymbol{k}_9^1=\pi(1,1,1)/a_0$	$\boldsymbol{k}_9^2=\pi(1,\bar{1},\bar{1})/a_0$	$\boldsymbol{k}_9^3=\pi(\bar{1},1,\bar{1})/a_0$	$\boldsymbol{k}_9^4=\pi(\bar{1},\bar{1},1)/a_0$

Table A1, together with the different stars of $\boldsymbol{k}$ (table A2), gives the symmetry modes necessary for describing the ionic positions in $P2_13$. In the first column the symbols for the symmetry coordinates are given. The third column denotes the point groups corresponding to the groups of $\boldsymbol{k}$ and the last column the irreps, both in Kovalev's and in the conventional notation.

Table A3. Symmetry modes of an octahedron.

$q(\mathrm{a_{1g}})$	$(x_1 + y_2 + z_3 - x_4 - y_5 - z_6)/\sqrt{6}$
$q(\mathrm{e_{g\theta}})$	$(2z_3 - x_1 - y_2 - 2z_6 + x_4 + y_5)\sqrt{12}$
$q(\mathrm{e_{g\epsilon}})$	$(x_1 - y_2 - x_4 + y_5)/2$
$q(\mathrm{t_{1g}}_x)$	$(z_2 - y_3 - z_5 + y_6)/2$
$q(\mathrm{t_{1g}}_y)$	$(x_3 - z_1 - x_6 + z_4)/2$
$q(\mathrm{t_{1g}}_z)$	$(y_1 - x_2 - y_4 + x_5)/2$
$q(\mathrm{t_{2g}}_{yz})$	$(z_2 + y_3 - z_5 - y_6)/2$
$q(\mathrm{t_{2g}}_{zx})$	$(x_3 + z_1 - x_6 - z_4)/2$
$q(\mathrm{t_{2g}}_{xy})$	$(y_1 + x_2 - y_4 + x_5)/2$
$q(\mathrm{t_{1u1}}_x)$	x_0
$q(\mathrm{t_{1u1}}_y)$	y_0
$q(\mathrm{t_{1u1}}_z)$	z_0
$q(\mathrm{t_{1u2}}_x)$	$(x_1 + x_4)/\sqrt{2}$
$q(\mathrm{t_{1u2}}_y)$	$(y_2 + y_5)/\sqrt{2}$
$q(\mathrm{t_{1u2}}_z)$	$(z_3 + z_6)/\sqrt{2}$
$q(\mathrm{t_{1u3}}_x)$	$(x_2 + x_3 + x_5 + x_6)/2$
$q(\mathrm{t_{1u3}}_y)$	$(y_1 + y_3 + y_4 + y_6)/2$
$q(\mathrm{t_{1u3}}_z)$	$(z_1 + z_2 + z_4 + z_5)/2$
$q(\mathrm{t_{2u}}_x)$	$(x_2 - x_3 + x_5 - x_6)/2$
$q(\mathrm{t_{2u}}_y)$	$(y_3 - y_1 + y_6 - y_4)/2$
$q(\mathrm{t_{2u}}_z)$	$(z_1 - z_2 + z_4 - z_5)/2$

A.2. Symmetric octahedron modes

In table A3 we give normalized octahedron modes which are orthogonal for the same site, but not necessarily orthogonal for adjacent sites. Table A3 consists of the modes of vibrations, translations and rotations of isolated octahedra each with a central atom. The numbering of the ligands follows the convention given by Van Vleck [27] (see figure 1). There are three $\mathrm{T_{1u}}$ modes, which can be expected to interact. However, our choice in this table leads to the simplest coordinates (similar ones have been used in [16, 5]). Table 5 gives the results for the different local coordinates.

A.3. Scalar invariants of the lower space group

In section 5, several bilinear quantities are derived. The values for these bilinear quantities differ for different types of site. These belong to scalar distributions, which can be classified as having irreps belonging to a specific $\boldsymbol{k}$-vector (referred to $Fm\bar{3}m$). These invariants of the space group of lower order are mentioned here for clarity. Their derivation is similar as that of the distortion modes which have been treated in subsection A.1.

$\mathcal{A}_1$ from equation (A1) is a constant, belonging to the Γ point. It describes ferrodistortive patterns of quantities like chirality and tetrahedral distortion, which are equal for all In ions or for all Cl ions. Note that invariants for $P2_13$ are not necessarily invariant in the B1 structure. We have

$$\mathcal{A}_1 = \text{constant} \tag{A1}$$

$$\mathcal{A}_2 = [\sin \boldsymbol{k}_4^1 \cdot \boldsymbol{r} + \sin \boldsymbol{k}_4^2 \cdot \boldsymbol{r} + \sin \boldsymbol{k}_4^5 \cdot \boldsymbol{r} + \sin \boldsymbol{k}_4^6 \cdot \boldsymbol{r} + \sin \boldsymbol{k}_4^9 \cdot \boldsymbol{r} + \sin \boldsymbol{k}_4^{10} \cdot \boldsymbol{r}] \tag{A2}$$

$$\mathcal{A}_3 = [\cos 2\boldsymbol{k}_6^1 \cdot \boldsymbol{r} + \cos 2\boldsymbol{k}_6^2 \cdot \boldsymbol{r} + \cos 2\boldsymbol{k}_6^3 \cdot \boldsymbol{r}] \tag{A3}$$

$$\mathcal{A}_4 = [\cos \boldsymbol{k}_9^1 \cdot \boldsymbol{r} + \cos \boldsymbol{k}_9^2 \cdot \boldsymbol{r} + \cos \boldsymbol{k}_9^3 \cdot \boldsymbol{r} + \cos \boldsymbol{k}_9^4 \cdot \boldsymbol{r}] \tag{A4}$$

$$\mathcal{A}_5 = [\sin \boldsymbol{k}_9^1 \cdot \boldsymbol{r} + \sin \boldsymbol{k}_9^2 \cdot \boldsymbol{r} + \sin \boldsymbol{k}_9^3 \cdot \boldsymbol{r} + \sin \boldsymbol{k}_9^4 \cdot \boldsymbol{r}]. \tag{A5}$$

Table A4. Coordinates of some specific In sites. (a_0 is the cubic rock-salt parameter.)

Coordinate	In(1) $(0.5, 0, 1.5)a_0$	In(2) $(1.5, 0, 0.5)a_0$
$q(\mathrm{a_{1g}})$	$-(4/3)s_1$	$(4/3)s_1$
$q(\mathrm{e_{g\theta}})$	$(2/3)\sqrt{2}s_1$	$-(2/3)\sqrt{2}s_1$
$q(\mathrm{e_{g\epsilon}})$	$-(2/3)\sqrt{6}s_2$	$(2/3)\sqrt{6}s_2$
$q(\mathrm{t_{1g}}x)$	$-(2/3)\sqrt{3}s_3 - (2/3)\sqrt{6}s_2$	$-(2/3)\sqrt{3}s_3 + (2/3)\sqrt{6}s_2$
$q(\mathrm{t_{1g}}y)$	$(\sqrt{6}/3)(d_1 - w_1)$	$(\sqrt{6}/3)(-d_1 + w_1)$
$q(\mathrm{t_{1g}}z)$	$-(\sqrt{6}/3)(d_1 + d_2 + w_1 - w_2)$	$(\sqrt{6}/3)(d_1 - d_2 + w_1 + w_2)$
$q(\mathrm{t_{2g}}yz)$	$(2/3)\sqrt{3}(s_3 + \sqrt{2}s_1)$	$(2/3)\sqrt{3}(s_3 - \sqrt{2}s_1)$
$q(\mathrm{t_{2g}}zx)$	$(\sqrt{6}/3)(d_1 - w_1 + 4l_2)$	$(\sqrt{6}/3)(-d_1 + w_1 + 4l_2)$
$q(\mathrm{t_{2g}}xy)$	$(\sqrt{6}/3)(-d_1 + d_2 - w_1 - w_2)$	$(\sqrt{6}/3)(d_1 + d_2 + w_1 - w_2)$
$q(\mathrm{t_{1u1}}x)$	$(\sqrt{6}/3)(-\sqrt{2}s'_3 + s'_1 - s'_2)$	$(\sqrt{6}/3)(\sqrt{2}s'_3 + s'_1 - s'_2)$
$q(\mathrm{t_{1u1}}y)$	$(\sqrt{6}/3)(-d'_2 + w'_2 + 2l'_1)$	$(\sqrt{6}/3)(d'_2 - w'_2 + 2l'_1)$
$q(\mathrm{t_{1u1}}z)$	$(\sqrt{6}/3)(d'_1 + d'_2 - w'_1 + w'_2)$	$(\sqrt{6}/3)(d'_1 - d'_2 - w'_1 - w'_2)$
$q(\mathrm{t_{1u2}}x)$	$-(2/3)\sqrt{6}s_3$	$(2/3)\sqrt{6}s_3$
$q(\mathrm{t_{1u2}}y)$	$-(2/3)\sqrt{3}(d_2 - w_2)$	$(2/3)\sqrt{3}(d_2 - w_2)$
$q(\mathrm{t_{1u2}}z)$	$(2/3)\sqrt{3}(d_1 + d_2 + w_1 + w_2)$	$(2/3)\sqrt{3}(d_1 - d_2 + w_1 - w_2)$
$q(\mathrm{t_{1u3}}x)$	$(\sqrt{6}/3)(s_1 - s_2)$	$(\sqrt{6}/3)(s_1 - s_2)$
$q(\mathrm{t_{1u3}}y)$	$-(\sqrt{6}/3)(d_2 + w_2)$	$(\sqrt{6}/3)(d_2 + w_2)$
$q(\mathrm{t_{1u3}}z)$	$(\sqrt{6}/3)(d_1 + d_2 - w_1 - w_2)$	$(\sqrt{6}/3)(d_1 - d_2 - w_1 + w_2)$
$q(\mathrm{t_{2u}}x)$	$(\sqrt{6}/3)(s_1 - s_2)$	$(\sqrt{6}/3)(s_1 - s_2)$
$q(\mathrm{t_{2u}}y)$	$(\sqrt{6}/3)(d_2 + w_2)$	$-(\sqrt{6}/3)(d_2 + w_2)$
$q(\mathrm{t_{2u}}z)$	$(\sqrt{6}/3)(d_1 - d_2 - w_1 + w_2)$	$(\sqrt{6}/3)(d_1 + d_2 - w_1 - w_2)$
Coordinate	In(3) $(0, 0, 0)a_0$	In(4) $(1, 1, 1)a_0$
$q(\mathrm{a_{1g}})$	$4l_2$	$-4l_2$
$q(\mathrm{e_{g\theta}})$		
$q(\mathrm{e_{g\epsilon}})$		
$q(\mathrm{t_{1g}}x)$	$-(\sqrt{6}/3)(d_2 + w_2 - \sqrt{2}s_3)$	$(\sqrt{6}/3)(d_2 + w_2 + \sqrt{2}s_3)$
$q(\mathrm{t_{1g}}y)$	$-(\sqrt{6}/3)(d_2 + w_2 - \sqrt{2}s_3)$	$(\sqrt{6}/3)(d_2 + w_2 + \sqrt{2}s_3)$
$q(\mathrm{t_{1g}}z)$	$-(\sqrt{6}/3)(d_2 + w_2 - \sqrt{2}s_3)$	$(\sqrt{6}/3)(d_2 + w_2 + \sqrt{2}s_3)$
$q(\mathrm{t_{2g}}yz)$	$(\sqrt{6}/3)(d_2 + w_2 + \sqrt{2}s_3)$	$-(\sqrt{6}/3)(d_2 + w_2 - \sqrt{2}s_3)$
$q(\mathrm{t_{2g}}zx)$	$(\sqrt{6}/3)(d_2 + w_2 + \sqrt{2}s_3)$	$-(\sqrt{6}/3)(d_2 + w_2 - \sqrt{2}s_3)$
$q(\mathrm{t_{2g}}xy)$	$(\sqrt{6}/3)(d_2 + w_2 + \sqrt{2}s_3)$	$-(\sqrt{6}/3)(d_2 + w_2 - \sqrt{2}s_3)$
$q(\mathrm{t_{1u1}}x)$	$(\sqrt{6}/3)((d'_1 + w'_1 + s'_1 + s'_2)$	$(\sqrt{6}/3)(-d'_1 - w'_1 + s'_1 + s'_2)$
$q(\mathrm{t_{1u1}}y)$	$(\sqrt{6}/3)(d'_1 + w'_1 + s'_1 + s'_2)$	$(\sqrt{6}/3)(-d'_1 - w'_1 + s'_1 + s'_2)$
$q(\mathrm{t_{1u1}}z)$	$(\sqrt{6}/3)(d'_1 + w'_1 + s'_1 + s'_2)$	$(\sqrt{6}/3)(-d'_1 - w'_1 + s'_1 + s'_2)$
$q(\mathrm{t_{1u2}}x)$	$(2/3)\sqrt{3}(d_1 - w_1)$	$(2/3)\sqrt{3}(-d_1 + w_1)$
$q(\mathrm{t_{1u2}}y)$	$(2/3)\sqrt{3}(d_1 - w_1)$	$(2/3)\sqrt{3}(-d_1 + w_1)$
$q(\mathrm{t_{1u2}}z)$	$(2/3)\sqrt{3}(d_1 - w_1)$	$(2/3)\sqrt{3}(-d_1 + w_1)$
$q(\mathrm{t_{1u3}}x)$	$(\sqrt{6}/3)(d_1 + w_1 + s_1 + s_2)$	$(\sqrt{6}/3)(-d_1 - w_1 + s_1 + s_2)$
$q(\mathrm{t_{1u3}}y)$	$(\sqrt{6}/3)(d_1 + w_1 + s_1 + s_2)$	$(\sqrt{6}/3)(-d_1 - w_1 + s_1 + s_2)$
$q(\mathrm{t_{1u3}}z)$	$(\sqrt{6}/3)(d_1 + w_1 + s_1 + s_2)$	$(\sqrt{6}/3)(-d_1 - w_1 + s_1 + s_2)$
$q(\mathrm{t_{2u}}x)$	$(\sqrt{6}/3)(d_1 + w_1 - s_1 - s_2)$	$(\sqrt{6}/3)(-d_1 - w_1 - s_1 - s_2)$
$q(\mathrm{t_{2u}}y)$	$(\sqrt{6}/3)(d_1 + w_1 - s_1 - s_2)$	$(\sqrt{6}/3)(-d_1 - w_1 - s_1 - s_2)$
$q(\mathrm{t_{2u}}z)$	$(\sqrt{6}/3)(d_1 + w_1 - s_1 - s_2)$	$(\sqrt{6}/3)(-d_1 - w_1 - s_1 - s_2)$

Table A5. Coordinates of some specific Cl sites.

Coordinate	Cl(1) $(1, 0, 1.5)a_0$	Cl(2) $(1, 0, 0.5)a_0$
$q(\mathrm{a_{1g}})$	$-(4/3)s_1'$	$(4/3)s_1'$
$q(\mathrm{e_{g\theta}})$	$-(\sqrt{2}/3)s_1' - \sqrt{2}s_2'$	$(\sqrt{2}/3)s_1' + \sqrt{2}s_2'$
$q(\mathrm{e_{g\epsilon}})$	$-(\sqrt{6}/3)s_1' + (\sqrt{6}/3)s_2'$	$(\sqrt{6}/3)(s_1' - s_2')$
$q(\mathrm{t_{1g}}x)$	$-(2/3)\sqrt{3}s_3' - (2/3)\sqrt{6}s_2'$	$-(2/3)\sqrt{3}s_3' + (2/3)\sqrt{6}s_2'$
$q(\mathrm{t_{1g}}y)$	$(\sqrt{6}/3)(d_1' + d_2' + w_1' + w_2')$	$(\sqrt{6}/3)(-d_1' + d_2' - w_1' + w_2')$
$q(\mathrm{t_{1g}}z)$	$(\sqrt{6}/3)(-d_2' + w_2')$	$(\sqrt{6}/3)(-d_2' + w_2')$
$q(\mathrm{t_{2g}}yz)$	$-(2/3)\sqrt{3}(s_3' + \sqrt{2}s_1')$	$-(2/3)\sqrt{3}(s_3' - \sqrt{2}s_1')$
$q(\mathrm{t_{2g}}zx)$	$(\sqrt{6}/3)(d_1' - d_2' + w_1' - w_2')$	$(\sqrt{6}/3)(-d_1' - d_2' - w_1' - w_2')$
$q(\mathrm{t_{2g}}xy)$	$(\sqrt{6}/3)(d_2' - w_2' - 4l_1')$	$(\sqrt{6}/3)(d_2' - w_2' + 4l_1')$
$q(\mathrm{t_{1u1}}x)$	$(\sqrt{6}/3)(-\sqrt{2}s_3 - s_1 - s_2)$	$(\sqrt{6}/3)(\sqrt{2}s_3 - s_1 - s_2)$
$q(\mathrm{t_{1u1}}y)$	$(\sqrt{6}/3)(-d_1 - d_2 - w_1 - w_2)$	$(\sqrt{6}/3)(-d_1 + d_2 - w_1 + w_2)$
$q(\mathrm{t_{1u1}}z)$	$(\sqrt{6}/3)(d_1 - w_1 + 2l_2)$	$(\sqrt{6}/3)(d_1 - w_1 - 2l_2)$
$q(\mathrm{t_{1u2}}x)$	$-2(\sqrt{6}/3)s_3'$	$2(\sqrt{6}/3)s_3'$
$q(\mathrm{t_{1u2}}y)$	$-(2/3)\sqrt{3}(d_1' + d_2' - w_1' + w_2')$	$(2/3)\sqrt{3}(-d_1' + d_2' + w_1' + w_2')$
$q(\mathrm{t_{1u2}}z)$	$(2/3)\sqrt{3}(d_1' + w_1')$	$(2/3)\sqrt{3}(d_1' + w_1')$
$q(\mathrm{t_{1u3}}x)$	$-(\sqrt{6}/3)(s_1' + s_2')$	$-(\sqrt{6}/3)(s_1' + s_2')$
$q(\mathrm{t_{1u3}}y)$	$(\sqrt{6}/3)(-d_1' - d_2' - w_1' + w_2')$	$(\sqrt{6}/3)(-d_1' + d_2' - w_1' - w_2')$
$q(\mathrm{t_{1u3}}z)$	$(\sqrt{6}/3)(d_1' - w_1')$	$(\sqrt{6}/3)(d_1' - w_1')$
$q(\mathrm{t_{2u}}x)$	$(\sqrt{6}/3)(s_1' + s_2')$	$(\sqrt{6}/3)(s_1' + s_2')$
$q(\mathrm{t_{2u}}y)$	$(\sqrt{6}/3)(-d_1' + d_2' - w_1' - w_2')$	$(\sqrt{6}/3)(-d_1' - d_2' - w_1' + w_2')$
$q(\mathrm{t_{2u}}z)$	$(\sqrt{6}/3)(d_1' - w_1')$	$(\sqrt{6}/3)(d_1' - w_1')$
Coordinate	Cl(3) $(0.5, 0.5, 0.5)a_0$	Cl(4) $(1.5, 1.5, 1.5)a_0$
$q(\mathrm{a_{1g}})$	$4l_1'$	$-4l_1'$
$q(\mathrm{e_{g\theta}})$		
$q(\mathrm{e_{g\epsilon}})$		
$q(\mathrm{t_{1g}}x)$	$(\sqrt{6}/3)(-d_1' + w_1' + \sqrt{2}s_3')$	$(\sqrt{6}/3)(d_1' - w_1' + \sqrt{2}s_3')$
$q(\mathrm{t_{1g}}y)$	$(\sqrt{6}/3)(-d_1' + w_1' + \sqrt{2}s_3')$	$(\sqrt{6}/3)(d_1' - w_1' + \sqrt{2}s_3')$
$q(\mathrm{t_{1g}}z)$	$(\sqrt{6}/3)(-d_1' + w_1' + \sqrt{2}s_3')$	$(\sqrt{6}/3)(d_1' - w_1' + \sqrt{2}s_3')$
$q(\mathrm{t_{2g}}yz)$	$(\sqrt{6}/3)(-d_1' + w_1' - \sqrt{2}s_3')$	$(\sqrt{6}/3)(d_1' - w_1' - \sqrt{2}s_3')$
$q(\mathrm{t_{2g}}zx)$	$(\sqrt{6}/3)(-d_1' + w_1' - \sqrt{2}s_3')$	$(\sqrt{6}/3)(d_1' - w_1' - \sqrt{2}s_3')$
$q(\mathrm{t_{2g}}xy)$	$(\sqrt{6}/3)(-d_1' + w_1' - \sqrt{2}s_3')$	$(\sqrt{6}/3)(d_1' - w_1' - \sqrt{2}s_3')$
$q(\mathrm{t_{1u1}}x)$	$(\sqrt{6}/3)(d_2 - w_2 - s_1 + s_2)$	$-d_2 + w_2 - s_1 + s_2$
$q(\mathrm{t_{1u1}}y)$	$(\sqrt{6}/3)(d_2 - w_2 - s_1 + s_2)$	$(\sqrt{6}/3)(-d_2 + w_2 - s_1 + s_2)$
$q(\mathrm{t_{1u1}}z)$	$(\sqrt{6}/3)(d_2 - w_2 - s_1 + s_2)$	$(\sqrt{6}/3)(-d_2 + w_2 - s_1 + s_2)$
$q(\mathrm{t_{1u2}}x)$	$(2/3)\sqrt{3}(d_2' - w_2')$	$(2/3)\sqrt{3}(-d_2' + w_2')$
$q(\mathrm{t_{1u2}}y)$	$(2/3)\sqrt{3}(d_2' - w_2')$	$(2/3)\sqrt{3}(-d_2' - w_2')$
$q(\mathrm{t_{1u2}}z)$	$(2/3)\sqrt{3}(d_2' - w_2')$	$(2/3)\sqrt{3}(-d_2' + w_2')$
$q(\mathrm{t_{1u3}}x)$	$(\sqrt{6}/3)(d_2' + w_2' - s_1' + s_2')$	$(\sqrt{6}/3)(-d_2' - w_2' - s_1' + s_2')$
$q(\mathrm{t_{1u3}}y)$	$(\sqrt{6}/3)(d_2' + w_2' - s_1' + s_2')$	$(\sqrt{6}/3)(-d_2' - w_2' - s_1' + s_2')$
$q(\mathrm{t_{1u3}}z)$	$(\sqrt{6}/3)(d_2' + w_2' - s_1' + s_2')$	$(\sqrt{6}/3)(-d_2' - w_2' - s_1' + s_2')$
$q(\mathrm{t_{2u}}x)$	$(\sqrt{6}/3)(-d_2' - w_2' - s_1' + s_2')$	$(\sqrt{6}/3)(d_2' + w_2' - s_1' + s_2')$
$q(\mathrm{t_{2u}}y)$	$(\sqrt{6}/3)(-d_2' - w_2' - s_1' + s_2')$	$(\sqrt{6}/3)(d_2' + w_2' - s_1' + s_2')$
$q(\mathrm{t_{2u}}z)$	$(\sqrt{6}/3)(-d_2' - w_2' - s_1' + s_2')$	$(\sqrt{6}/3)(d_2' + w_2' - s_1' + s_2')$

$\mathcal{A}_2$ gives opposite values for In(1) and In(2), and similarly for Cl(1) and Cl(2) (the type of ion is denoted in the brackets). $\mathcal{A}_3$ gives values in proportion to $-1, -1, 3, 3$ for In of the first to the fourth type, respectively. This is also the case for the Cl ions. $\mathcal{A}_4$ gives opposite values for In(3) and In(4) and $\mathcal{A}_5$ gives opposite values for Cl(3) and Cl(4).

A.4. Displacements at specific sites expressed in normal lattice coordinates

In this subsection the moments at specific In and Cl sites are given in terms of the normal coordinates. This serves to derive the Landau third-order invariants. Tables A4 and A5 can serve also for deriving the bilinear quantities, which transform as A_{1g}, A_{1u}, A_{2u} and A_{2g}. The squares of these quantities result in fourth-order invariants expressed in symmetry coordinates. This applies also to the real symmetry coordinates as in the so-called geometric approximation. For the latter, a quicker way of obtaining these results is by means of table 5.

References

[1] Van den Berg J M 1964 *Thesis* Leiden University
[2] Van den Berg J M 1966 *Acta Crystallogr.* **20** 905–10
[3] Van der Vorst C P J M, Verschoor G C and Maaskant W J A 1980 *Acta Crystallogr.* B **34** 3333–5
[4] Van der Vorst C P J M and Maaskant W J A 1980 *J. Solid State Chem.* **34** 301–13
[5] Maaskant W J A 1993 *New J. Chem.* **17** 97–105
[6] Wyckoff R W G 1963 *Crystal Structures* 2nd edn, vol 1 (New York: Interscience)
[7] Goldak J, Barrett C S, Innes D and Youdelis W 1966 *J. Chem. Phys.* **44** 3323–5
[8] Lines M E and Glass A M 1977 *Principles and Applications of Ferroelectric and Related Materials* (Oxford: Clarendon)
[9] Alcock N W and Jenkins H D B 1974 *J. Chem. Soc. Dalton Trans.* 1907–11
[10] Leciejewicz J 1961 *Acta Crystallogr.* **14** 66
[11] Kay M I 1961 *Acta Crystallogr.* **14** 80–1
[12] Van Arkel A E 1961 *Moleculen en Kristallen* (Gravenhage: Van Stockum & Zoon) p 134
[13] Krebs H 1968 *Inorganic Crystal Chemistry* (London: McGraw-Hill) pp 199–200
[14] Landau L D 1937 *Sov. Phys.–JETP* **7** 627
Landau L D 1937 *Phys. Z. Sowjetunion* **11** 545–55 (Engl. Transl. 1965 *Collected Papers of Landau* ed D Ter Haar (London: Gordon and Breach))
[15] Landau L D and Lifshitz E M 1980 *Statistical Physics* vol 5, part I (Oxford: Pergamon) pp 459–71
[16] Van der Vorst C P J M 1981 *J. Phys. Chem. Solids* **42** 655–65
[17] Condon E U 1937 *Rev. Mod. Phys.* **9** 431–57
[18] Watanabe H 1966 *Operator Methods in Ligand Field Theory* (Englewood Cliffs, NJ: Prentice-Hall)
[19] Maaskant W J A and Haije W G 1986 *J. Phys. C: Solid State Phys.* **19** 5295–308
[20] Tolédano J C and Tolédano P 1987 *The Landau Theory of Phase Transitions* (Singapore: World Scientific)
[21] Stokes H T and Hatch D M 1988 *Isotropy Subgroups of the 230 Crystallographic Space Groups* (Singapore: World Scientific)
[22] Haas C 1965 *Phys. Rev.* **140** A863–8
[23] Goodenough J B and Longo J M 1970 *Landolt–Börnstein New Series* Group III, vol 4 (Berlin: Springer) ch 3
[24] *Space Group Symmetry (International Tables for Crystallography A)* 1995 ed T Hahn (Dordrecht: Kluwer)
[25] Bradley C J and Cracknell A P 1972 *The Mathematical Theory of Symmetry in Solids* (Oxford: Clarendon)
[26] Kovalev O V 1961 *Irreducible Representations of the Space Groups* 2nd edn, ed H T Stokes and D M Match (New York: Gordon and Breach)
[27] Van Vleck J H 1939 *J. Chem. Phys.* **7** 72–84